Clinical Spectroscopy 3 (2021) 100012

Contents lists available at ScienceDirect

Clinical Spectroscopy

journal homepage: www.sciencedirect.com/journal/clinical-spectroscopy

# Intra-operative Raman spectroscopy and *ex vivo* Raman mapping for assessment of cartilage degradation

Riana Gaifulina [a,b], Abigail D.G. Nunn [a], Edward R.C. Draper [c], Robin K. Strachan [d], Nathan Blake [e], Steven Firth [b], Geraint M.H. Thomas [e], Paul F. McMillan [b,*], Jayesh Dudhia [a,*]

[a] Department of Clinical Science and Services, Royal Veterinary College, University of London, Hawkshead Lane, Hatfield, AL9 7TA, UK
[b] Department of Chemistry, University College London, Gordon Street, London, WC1H 0AJ, UK
[c] Department of Materials Science and Engineering, University of Sheffield, Mappin Street, Sheffield, S1 3JD, UK
[d] Imperial College Healthcare NHS Trust, Charing Cross Hospital, Fulham Palace Road, London, W6 8RF, UK
[e] Department of Cell and Developmental Biology, University College London, Gower Street, London, WC1E 6AP, UK

ARTICLE INFO

*Keywords:*
Articular cartilage
Osteoarthritis
Raman spectroscopy
Raman mapping
Arthroscopy
Glycosaminoglycans

ABSTRACT

The development of a label-free, non-destructive and safe analytical method such as Raman spectroscopy for assessing cartilage degradation is highly desirable. Compared to non-optical imaging modalities, Raman mapping offers a more sensitive means of directly assessing the chemical composition of cartilage in three-dimensional space and the potential to monitor cartilage degeneration to inform intervention and treatment strategies. Herein, we report the application of Raman spectroscopic methods *ex vivo* and at arthroscopy to identify molecular alterations in cartilage specimens containing minor focal lesions characteristic of the early disease phase. Our initial *ex vivo* analysis, obtained by single-point Raman spectroscopy of cartilage samples, supports previous findings based on S-O stretching vibration bands associated with sulphated glycosaminoglycans (sGAGs). We extended the analyses to the high-wavenumber region where we observed that vibrational bands assigned to C-H and O-H stretching modes discriminated early cartilage alterations from healthy cartilage samples. Furthermore, we performed a proof-of-concept in-clinic study using a custom-built optical probe to acquire Raman spectral measurements for the first time in patients undergoing arthroscopy of knee joints. Spectra were obtained with adequate signal-to-noise ratios that similarly discriminated between lesion and adjacent cartilage sites and identified reductions in sGAGs in apparently healthy cartilage. Building on this, we present initial results from Raman mapping to spatially resolve the molecular constituents of cartilage through its depth and across a lesion. Mapping revealed a non-uniform and reduced sGAG distribution within the lesion and peripheral cartilage that was otherwise visually normal, similar to the in-clinic observations, showing that the degradative influence of the lesion extended beyond its border. This was accompanied by a decreased fluorescence signal intensity, which suggests that fluorescence may provide valuable information as an adjunct to the Raman signal in discriminating normal and degenerating cartilage. This work demonstrates the value of Raman mapping over single-point Raman measurements for the analysis of the anisotropy of articular cartilage and highlights the potential of the technology for *in vivo* articular joint arthroscopy applications.

## 1. Introduction

Diarthrodial joints are dependent on a thin layer of hyaline cartilage at their bony surfaces that enables near-frictionless movement and dissipation of the mechanical loads experienced during locomotion. Articular cartilage is a highly specialised tissue and structural lesions (fibrillations) that occur at its surface do not readily heal [1,2]. Such fibrillar lesions are considered to progress to osteoarthritis (OA), a disease characterised by the progressive loss of a smooth articulating surface, pain, remodelling of joint tissues and eventual biomechanical failure of the joint [3,4]. OA is the leading cause of chronic disability in the elderly, with the knee and hip being most commonly involved, but it

*Abbreviations:* OA, osteoarthritis; ECM, extracellular matrix; PG, proteoglycan; GAG, glycosaminoglycan; sGAG, sulphated glycosaminoglycan; MRI, magnetic resonance imaging; ICRS, International Cartilage Repair Society.

* Corresponding authors.
*E-mail addresses:* p.f.mcmillan@ucl.ac.uk (P.F. McMillan), jdudhia@rvc.ac.uk (J. Dudhia).

https://doi.org/10.1016/j.clispe.2021.100012
Received 24 March 2021; Received in revised form 13 May 2021; Accepted 5 June 2021
Available online 7 June 2021
2666-0547/© 2021 The Authors. Published by Elsevier B.V. This is an open access article under the CC BY license (http://creativecommons.org/licenses/by/4.0/).

can also affect other articular joints [5]. Worldwide it is estimated that 9.6% of men and 18.0% of women over 60 years of age have symptomatic OA, with approximately 80% of those experiencing limitations in joint movement and debilitating pain. Currently, no disease-modifying therapies exist.

The characteristic physicochemical properties of articular cartilage are due to the highly ordered anisotropic structural organisation of its extracellular matrix (ECM), and variations in the distribution of chondrocytes and the molecular constituents of cartilage with depth have been reported [6]. Cartilage is generally subdivided into three structural zones based on the orientation of its collagen type II fibrils [7]. The major functional interactions occur between the two most abundant protein components, collagen type II and aggrecan. Aggrecan is a large proteoglycan (PG) that is densely substituted with sulphated glycosaminoglycan (sGAG) moieties. Fibrillar collagen forms a network that provides elastic restraint, whereas aggrecan is responsible for sustaining tissue hydration, which is necessary for compressive resilience, through the osmotic swelling pressure indirectly generated by the polyanionic sulphate (-$OSO_3$-/-$OSO_3$OH) group [8,9]. Cartilage function is compromised by elastic weakening due to proteolytic cleavage of the collagen network resulting in fibrillation of the cartilage surface. Consequently, large structural alterations of the ECM occur, and these are considered to mark the point at which irreversible loss of cartilage commences [3,10]. It has been established *via* biochemical analysis that the earliest stages of OA are associated with aggrecan loss along with increased tissue hydration [11–14] and are considered to be reversible [15–17]. Intervention might prevent progressive cartilage damage if early disease stages could be identified. However, accurately identifying early molecular changes has proved challenging with the currently available methodology, and this hinders the development of disease-modifying OA drugs and other early-intervention treatment regimes. Of value would be the development of a spectroscopic technique calibrated to detect the biochemical and structural changes that occur prior to overt fibrillation of cartilage.

X-ray transmission radiographic imaging is typically applied to diagnose OA by identifying narrowing of the articular joint space as an obvious indicator of cartilage erosion. The sensitivity of this approach is therefore limited to late disease stages, once significant and irreversible deterioration has already occurred [18]. Magnetic resonance imaging (MRI) provides direct morphological assessment of cartilage [19], with recent advances in contrast agents enabling quantitative biochemical approaches for imaging spatial distributions of PGs, tissue hydration and collagen organisation [20–23]. However, standard MRI techniques are not used routinely in the clinic due to cost considerations. Furthermore, incomplete penetration into the cartilage of the paramagnetic contrast agent necessary for quantitative imaging can hinder PG quantification [20]. Advances in developing and applying quantitative MRI (qMRI) techniques to assess cartilage damage and correlate these with changes in biochemical and biomechanical properties are progressing rapidly, although much of the work remains at an experimental stage [24,25]. Studies to develop predictive biomarkers for cartilage metabolites released into the circulation or synovial fluid have yielded promising results but these too remain to be fully validated [26,27].

Optical imaging and spectroscopic techniques are increasingly being developed to play a role in early assessment of cartilage disease and damage. These include optical coherence tomography (OCT) coupled with qMRI to yield through-depth characterization of the tissue [28]. Label-free second harmonic generation microscopy can provide additional detail on specific molecular components within the tissue [29]. However, although pathways exist for the *in vivo* implementation of these advanced optical techniques during surgery or pre-clinical assessment, they remain in the early stages of development. Determining suitable non-invasive markers of morphological and biochemical changes at the molecular level for early-stage cartilage disease that might facilitate the development of pharmaceutical treatment or provide better control over surgical intervention remains an important goal in the field [30].

The potential of optical spectroscopic techniques for the study of osteoarthritis at arthroscopy has recently been explored. For example, near-infrared spectroscopy has been demonstrated as a method for *in vivo* assessment of the biomechanical properties of equine cartilage [31]. Raman spectroscopy has been shown to be capable of identifying systematic changes in the vibrational spectra and relative intensities of specific biomarkers in cartilage biopsy samples correlated with International Cartilage Repair Society (ICRS) OA grades [32–35]. Raman spectroscopy is a light scattering technique in which characteristic energy shifts (expressed in wavenumber units, $cm^{-1}$) of an incident laser beam occurring as a result of interactions with vibrational modes of chemical species are measured. Thus, Raman spectroscopic analyses of biological specimens can be used to identify molecular signatures. Specific shifts associated with the primary macromolecular components of cartilage – collagen and aggrecan – have been identified in the spectra of excised cartilage samples [36]. sGAGs give rise to a characteristic band in the Raman spectrum in the 1060–1070 $cm^{-1}$ range due to S-O stretching vibrations of the -$OSO_3$-/-$OSO_3$OH groups [36,37]. Initial studies in this area by us and others demonstrated a systematic intensity decrease for this band in the spectra of samples with progressively more severe OA classifications, indicating its potential value for assessing early-phase compositional changes within cartilage [32–35]. Other relevant Raman bands include those at 1380 $cm^{-1}$ and 1424 $cm^{-1}$, which have been tentatively assigned to $CH_3$ and COO- vibrations, respectively, of GAGs [38]. However, within the field of osteoarthritis research, analyses of Raman data outside the fingerprint region of the vibrational spectrum, in the high-wavenumber region, are lacking.

In this study our first aim was to verify the validity of the use of the sGAG Raman band at 1063 $cm^{-1}$ in determining the degeneration state of *ex vivo* human cartilage. The second aim was to evaluate the biochemical data encoded in the high-wavenumber region of the Raman spectrum by multivariate data analysis to identify clinically valuable systematic changes associated with cartilage degradation. Furthermore, we aimed to test the applicability of Raman spectroscopy at knee arthroscopy in patients. Because both the incident laser beams and Raman scattered photons have wavelengths in the visible-to-near-IR region of the spectrum, they can be readily focused on and collected from the sampling region of interest, including *via* specially designed arthroscopic probes based on fibre optics that can be implemented for intraoperative assessment during orthopaedic interventions [34,39]. Applying these principles, we were able to extend our observations to include initial results obtained during exploratory arthroscopic surgery. Finally, we demonstrated the value of Raman mapping techniques in spatially resolving molecular constituents of cartilage throughout its depth, overcoming the limitations of current techniques based on micron-order tissue sampling and establishing the importance of mapping across larger tissue areas.

## 2. Materials and methods

### 2.1. Biopsy sample preparation

Cartilage samples from human femoral condyles were obtained following institutional ethics approval (Stanmore Musculoskeletal Biobank, REC 09/H0304/78; RVC Ethics and Welfare Committee, URN 2016 1467). Cartilage specimens for the *ex vivo* single-point spectroscopy study were collected within 18 h following lower-limb amputation for osteosarcomas from knee joints not involved in the tumour pathology. Those with an intact surface and glossy appearance without any macroscopic lesions (ICRS grade 0) were categorised as normal (control) specimens ($n$ = 3, 36–60 years). Occasionally, in some of these apparently healthy knee joints, small partial-thickness focal lesions of ~0.5–2 $cm^2$, which have been shown to exhibit characteristics of the biochemical changes seen in OA [40], were observed in the cartilage. Cartilage samples from these were taken from sites adjacent and distal to the

lesion (Supplementary Fig. 1a). In some instances, normal cartilage and cartilage with lesions was sampled from the same specimen for the single-point Raman spectroscopy study (Supplementary Table 1). Cartilage specimens with lesions were classified as degenerative, with those having either a small area of surface roughening with loss of glossy appearance as grade 1 ($n = 3$, 36–66 years) or those with a partial-depth erosion as combined grades 2/3 ($n = 4$, 38–66). Residual cartilage specimens from total knee replacement ($n = 2$, 59 and 68 years) were also analysed and classified as late-stage OA (grade 4). An additional grade 4 sample (66 years) was used for the biochemical assays.

Full-depth cartilage specimens were prepared to include the synovial surface and subchondral bone. Specimens were washed in Dulbecco's modified Eagle's medium (Thermo Fisher Scientific Inc., UK) to remove residual synovial fluid and blood before biochemical analysis, snap-freezing for histology or storage at –80 °C until experimental analysis. Specimens were prepared for biochemical analysis of sGAG and water content (with the subchondral bone removed), as well as for histology and Raman microspectroscopy. Full-depth cartilage specimens used for Raman spectroscopy mapping studies were embedded in optimal cutting temperature compound (Tissue-Tek® O.C.T.™, Sakura Finetek Europe B.V., Netherlands). Cryosections of 20 μm thickness were mounted on super mirror stainless steel slides (Thames Stockholders Ltd, Middlesex, U.K.) that had been previously shown to be Raman compatible [41,42] and the optimal cutting compound was removed using deionised water prior to Raman spectroscopy or imaging.

### 2.2. Biochemical assay and histological staining

sGAG assays were performed on specimens of full-depth cartilage (approximately 10–50 mg) ICRS G0 ($n = 3$), G1 ($n = 3$), G2/3 ($n = 4$) and G4 ($n = 3$) specimens (Table 1). The cartilage was cut into 20 μm cryosections and proteoglycans were extracted with 10 volumes of buffer (4 M guanidium chloride, 50 mM sodium acetate, 10 mM EDTA, pH 6.8) for 24 h at 4 °C and cleared extracts were assayed for sGAG using the dimethylmethylene blue method [43]. Snap-frozen cartilage was cryosectioned at 5 μm (Bright cryostat), and then stained with safranin O. Water content was measured by tissue weight before and after lyophilisation of samples for 24 h (Heto Maxi Dry, Thermo Scientific). An unpaired Student's t-test was applied for the statistical analysis and a $p$ value of 0.05 or less was considered significant.

### 2.3. Raman microspectroscopy

#### 2.3.1. Single-point spectroscopy of synovial surface of cartilage biopsies

An inVia Raman microspectroscopy instrument (Renishaw plc, Wotton-under-Edge, UK) equipped with a 785 nm laser was used for our initial studies of excised cartilage tissue as well as for acquisition of collagen and aggrecan samples [33,44]. The choice of near-IR laser excitation for such measurements has been discussed previously [34,35,44]. The incident beam was focused on the synovial surface of the sample to collect data using a Leica 50×/0.5 N.A. long working distance microscope objective. The laser power was measured to be ~15 mW at the sample, which is sufficiently low to avoid laser-induced degradation. Four spectral acquisitions (15 min total collection time) were averaged for each sample. In initial experiments, cartilage samples were immersed in synovial fluid or deionised water during measurements to assess the influence of the use of different fluids on spectral acquisition. The influence of freezing was also examined by comparing spectra from fresh cartilage samples and samples thawed following −80 °C storage. No major differences between these spectra were observed (Supplementary Fig. 2) and all subsequent *ex vivo* spectral acquisition was carried out in water after thawing stored frozen cartilage.

**Table 1**
Biochemical analyses of sGAG and water contents in cartilage samples.

| Grade[g] | Total sGAG[h] Content (μg/mg dry wt.)[i] | Water Content (% dry wt.)[i] |
|---|---|---|
| G0 ($n = 3$) | 140.2 ± 18.2 | 73.1 ± 0.95 |
| G1 ($n = 3$) | 132.0 ± 12.4 | 71.2 ± 0.80 |
| G2/3 ($n = 4$) | 102.8 ± 18.7* | 78.6 ± 1.25* |
| G4 ($n = 3$) | 92.0 ± 22.1* | 77.2 ± 1.86** |

* $p < 0.05$ for the difference from grade 0.
** $p < 0.05$ for the difference from grades 0 and 1.
[g] G0 to G4 denote grades 0 to 4.
[h] sGAG, sulphated glycosaminoglycan.
[i] Values represent mean ± 1 s.d.

#### 2.3.2. Raman mapping of full-depth cartilage sections

Raman imaging of excised cartilage tissue sections was carried out using the Renishaw StreamLine™ image acquisition tool within a RA816 Biological Analyser system equipped with imaging capability (Renishaw plc, Wotton-under-Edge, UK). Maps were obtained covering the full depth of cartilage from three locations: 1) within a lesion area, 2) adjacent to the lesion and 3) distal site to the lesion (apparently normal cartilage) from a 47 year specimen (Supplementary Fig. 1a). The lesion map consisted of 30,530 individual spectra, acquired using a 20 μm step size, encompassing most of the eroded surface over the full cartilage depth, extending into the subchondral bone. Smaller maps of the adjacent and distal sites consisted of approximately 15,000 individual spectra acquired using a 3 μm step size. Maps were also obtained for cartilage sampled from a joint with no lesions as a control (18 years) which consisted of approximately 19,000 individual spectra. All maps were acquired using a 785 nm laser line and 50×/0.75 N.A. short working distance objective delivering 158 mW of laser power onto the sample surface over a pixel dwell time of 3 s. A significantly higher laser power was used for the mapping studies compared to the point measurements because during mapping the laser beam was line focused such that it illuminated a large surface area of the sample; thus the optical power density at the sample remained low, reducing the likelihood of photothermal degradation. The RA816 system was limited to the 0–3000 $cm^{-1}$ Raman shift range and hence we were unable to image the high-wavenumber region extending beyond 3000 $cm^{-1}$.

### 2.4. Reference Raman spectra from laboratory-grade chemicals

Reference Raman spectra representative of the main cartilage constituents were collected from chondroitin sulphate A sodium salt, collagen and synthetic hydroxyapatite (Sigma-Aldrich Inc. Dorset, UK) using a Renishaw R816 Biological Analyser A total of five spectra were acquired for each chemical sample from different areas within the sample, using a 10 s acquisition time per measurement, and then an average was taken across all the measurements to obtain the reference spectrum.

### 2.5. Arthrospectroscopic in-clinic studies

#### 2.5.1. Optical probe design

For implementation of the Raman spectroscopy technique during surgical procedures, an optical probe was engineered to deliver and focus the incident laser and collect the Raman scattered signal from the region of interest. The probe was designed to be compatible with techniques and instrumentation used for knee arthroscopy (Supplementary Fig. 3). The aim was to transmit laser light from an optical fibre to the end of a 6 mm outer-diameter steel cylinder that could be used as an arthroscopic tool to deliver the laser beam onto the cartilage surface within the knee and collect the backscattered photons.

The optical probe was machined from 316 L S16 steel with a main body length of 100 mm to include a threaded connector, a sapphire lens (Edmund Optics, UK) to focus the laser beam and an endcap with a 4.5 mm diameter sapphire window (Edmund Optics, UK) (Supplementary Fig. 3a). The lens was positioned within the probe such that the focal point of the laser was at the exit of the sapphire window, enabling focus-

free use of the probe at arthroscopy. Both full-ball and half-ball lensing solutions were initially trialled in *ex vivo* experiments, with best results obtained using a single full-ball lens designed to deliver 15–30 mW of laser power to the sample surface. The lens and sapphire window were fixed in position with Loctite M31-CL epoxy adhesive (Henkel Ltd, Herts, UK), which meets the ISO 10993 biocompatibility standard for medical devices and is resistant to ethylene oxide sterilisation. The probe was coupled to a Renishaw inVia system with 785 nm laser excitation and fibre optic delivery for initial trials (Supplementary Fig. 3b).

#### 2.5.2. In-clinic investigation

Implementation of the probe was first optimized on cadaver joint specimens under research ethical approval obtained from the Integrated Research Application System (IRAS) (10/H0711/2) and the RVC Ethics and Welfare Committee (2010 0004 H). The main aim was to determine that spectra with acceptable signal-to-noise characteristics could be acquired both within a reasonably short time, to minimize the burden on patient and surgeon (i.e., less than 2 min per collection point), and within the constraints of an optical probe that had a size and shape compatible with standard arthroscopic surgical procedures. These initial experiments enabled the manipulation and familiarisation of the hand-held optical arthroscopy probe by the surgeon for positioning within the knee joint. The window of the probe was carefully abutted against the cartilage at specific locations on the femoral condylar cartilage before the arthroscope light was switched off for acquisition of Raman spectra. These experiments also allowed us to determine the optimal conditions for spectral acquisition and verify the minimum time for acquisition of spectra with reasonable signal-to-noise levels without burden to the patient or surgeon (2 min). Spectra were obtained under minimal room lighting conditions, with the operating theatre lights switched off. Interference from background lighting (essential theatre instruments and video monitors) was minimised by using blackout drapes to cover the spectral acquisition area immediately before spectra were acquired.

Following measurement optimisation, four patients undergoing exploratory arthroscopy of the knee for suspected cartilage defects were recruited following informed consent and study approval (Imperial College NHS Trust Research Ethics Committee 10/H0711/2). The cartilage lesions observed at arthroscopy were visually graded using the Outerbridge classification [45] (Supplementary Table 2). The probes underwent ethylene oxide sterilisation before Raman spectroscopy measurements were performed at arthroscopy for each patient under Hartmann saline lavage and distension of the knee joint, with the camera portal light as well as theatre and non-essential instrument lighting switched off (Supplementary Fig. 3c). Interference from essential lighting was minimised by covering the spectral acquisition area with blackout drapes during the acquisition. All joints exhibited an area of partial erosion of the femoral condyle cartilage of approximately of 4 to 6 $cm^2$. A series of spectra with acquisition times of 2 min each were obtained from two sites: (i) within fibrillated cartilage and (ii) at a distance of 10–15 mm from the fibrillating cartilage within the adjacent macroscopically normal cartilage. The effect of the theatre and instrument lighting was evaluated prior to these measurements.

### 2.6. Analysis

#### 2.6.1. Pre-processing

Cosmic ray artefacts were first removed from all datasets using the zap feature within the WiRE 5 software package (Renishaw plc, Wotton-under-Edge, UK). Raman spectra of cartilage sections were initially collected over a range of spectral shifts from the incident laser line from ~40–4000 $cm^{-1}$. For the data analysis, the spectra were typically segregated into two regions: (i) the fingerprint region (450–1800 $cm^{-1}$) and (ii) the high-wavenumber region (2500–4000 $cm^{-1}$). Spectra were then imported into Matlab R2017a (MathWorks, Natick, MA, USA), baseline corrected using the adaptive min-max routine described by Cao et al. [46] and vector normalised such that the intensity at each frequency in the spectrum was divided by the square root of the sum of the squares of all the intensities, where the sum was over all frequencies [46]. The adaptive min-max method was implemented as it has previously been shown to provide significantly better results than any single polynomial fit and is more amenable to implementation in an automated real-time *in vivo* Raman platform. The Raman mapping datasets underwent the same pre-processing steps. Spectra acquired *in vivo* during in-clinic tests underwent an additional smoothing step using a Savitzky–Golay filter with a smoothing window of 11 and a second-order polynomial.

#### 2.6.2. Empirical data analysis

Our initial detailed analysis of the spectral region of interest (ROI) spanning 985–1120 $cm^{-1}$ was aimed at examining systematic variations in the intensity of the sulphate (-$OSO_3$-) S-O stretching band at 1063 $cm^{-1}$ calibrated against the intensity of the dominant sharp band at 1003 $cm^{-1}$ assigned to phenylalanine residues; these two bands are common to both the collagen and aggrecan components of cartilage. Within the broader spectral band between 985 and 1120 $cm^{-1}$, we fitted seven subbands to mixed Gaussian−Lorentzian functions using the WiRE 5.0 software (Renishaw plc, Wotton-under-Edge, UK). Each subband was identified using Savitzky–Golay differentiation filtering with a second-order polynomial and first-order derivative. Subband areas were then exported into a spreadsheet and band area ratios $A_{1063}/A_{1003}$ were calculated by dividing the 1063 $cm^{-1}$ band area by the 1003 $cm^{-1}$ band area for each specimen. The same approach was applied to the analysis of the spectra obtained during *in vivo* investigations. For the statistical analysis of the groups, one-way ANOVA was applied (non-parametric, Kruskal–Wallis test). Dunn's multiple comparison post-test was carried out to determine statistically significant differences between groups. A $p$ value of 0.05 or less was considered significant in all statistical tests.

#### 2.6.3. Multivariate data analysis

A multivariate approach was applied to the same spectral datasets used in the initial examination of the spectral ROI described above, but in this case the entire recorded wavenumber range was considered. Difference spectra were computed and principal component analysis (PCA) was carried out in MATLAB using the IRootLab toolbox [47]. Difference spectra were obtained by averaging the spectra for each OA grade and subtracting the normal (grade 0) spectrum as a reference point from each grade. PCA was used to evaluate the factors affecting the spectral variation across the sample groups. This analysis was based on the correlation matrix of the original dataset and involved the rotation of the data matrix such that a new set of principal component axes (PCs) were produced to maximise the variance within the dataset [48]. With this approach the largest variance lies on the first axis, and the variance decreases thereafter for each successive axis. As a result PCA enables the separation of sample groups based explicitly on their unique biochemical profile.

Full-depth Raman maps obtained from cartilage sections were analysed using the WiRE 5.0 software and heat maps showing the fluorescence and sGAG distributions were generated from each specimen dataset. The tissue fluorescence was quantified as the total area under the Raman spectral bands that had been extracted from the raw Raman spectra as background. To gain an insight into the spatial distribution and general abundance of sGAG, direct classical least squares (DCLS) component analysis was used. This algorithm approximates the spectrum at each point in the map by summing together scaled copies of each input reference spectrum. Given that this approach requires that reference spectra for all components in the sampled mixture are used as inputs, we inputted spectra of the most abundant (non-aqueous) components of articular cartilage – collagen, aggrecan (chondroitin sulphate sodium salt) and hydroxyapatite. An optimal cutting compound reference spectrum was also used as contamination from histological processing was observed. Water was not used as a reference input as dry tissue sections were imaged in this part of the study.

## 3. Results and discussion

### 3.1. Examining relative intensity changes in the sGAG characteristic Raman band with cartilage degeneration

Spectra from points across the synovial surface of cartilage specimens were recorded over the Raman shift range of 200 to 4000 $cm^{-1}$ (Fig. 1a). These consisted of a series of bands in the fingerprint region, at approximately 400–1800 $cm^{-1}$, characteristic of the collagen, aggrecan and other components of cartilage [44]. In addition, in the high-wavenumber region, we observed a broad O-H stretching band at ~3250 $cm^{-1}$ due to the presence of molecular water incorporated into the tissue and an aliphatic C-H stretching band slightly below 3000 $cm^{-1}$.

Following baseline subtraction, systematic changes in the relative band intensities occurring as a function of cartilage degradation became more apparent (Fig. 1b). Our initial investigation focused on the 1063 $cm^{-1}$ S-O stretching band of sGAG, which is an abundant moiety of aggrecan that is known to be lost in the early phases of cartilage degradation [10,11]. The intensity of this band decreased with increasing cartilage degeneration. This observation was consistent with the biochemical analysis of cartilage specimens (Table 1) and the histology of tissue samples prepared from normal and lesion-site cartilage (Supplementary Fig. 1b). It was also apparent that the intensity of the 1063 $cm^{-1}$ band decreased relative to those of the other bands in the spectrum with lesion grade (Fig. 1b), suggesting a decrease in the sGAG moiety. To quantify the relative intensity changes, the 985–1120 $cm^{-1}$ region was curve fitted using a series of mixed Gaussian−Lorentzian functions (Fig. 1c). The results of the Kruskal−Wallis test were significant ($H = 16.9$, 3 d.f., $p = 0.0007$), indicating a statistically significant difference between the lesion grades. Although there appeared to be a systematic decrease in the $A_{1063}/A_{1003}$ band area ratio with increasing lesion grade, pairwise comparisons using Dunn's post-hoc tests indicated statistically significant differences only between grades 0 and 4 ($p = 0.01$), grades 1 and 4 ($p = 0.00004$) and grades 2/3 and 4 ($p = 0.03$) (Fig. 1d). An overall decrease in the $A_{1063}/A_{1003}$ ratio from 1.69 (grade 0) to 0.99 (grade 4) was observed, which indicates that this ratio has potential value as a marker for advanced degeneration state. However, the ability to distinguish between normal cartilage and cartilage from late-stage disease has limited clinical value because advanced disease can be readily diagnosed by alternative imaging modalities such as radiology or MRI. Thus, a univariate data analysis approach utilising a single band ratio may be insufficient to identify earlier stages of disease.

Whereas it was possible to use the $A_{1063}/A_{1003}$ band area ratio to discriminate grade 4 cartilage from each of the other cartilage grades, a number of underlying data processing limitations hinder the use of this approach to assess the degree of cartilage deterioration. First, there are no standardised methods for pre-processing Raman spectra of biological origin, and this is particularly problematic with regard to baseline correction methods [46,49,50]. Baseline 'over-correction' can critically alter underlying spectral profiles, changing band heights and widths [51]. Overcorrection by subtracting a polynomial of order greater than

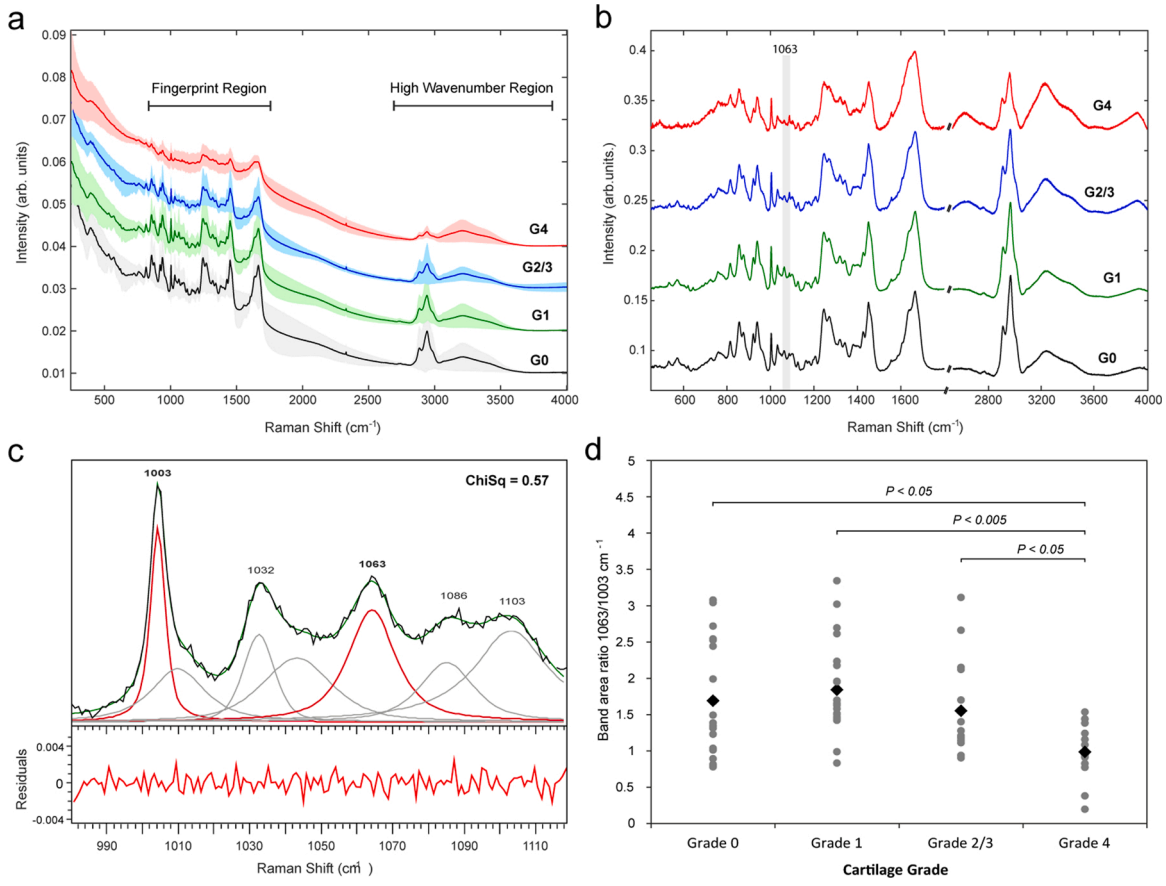


**Fig. 1.** Raman spectra acquired from cartilage specimens. Macroscopically normal cartilage and cartilage with small focal lesions underwent single-point Raman spectroscopic analysis. The spectra shown are averages of a minimum of three acquisitions. a) Averaged Raman spectra obtained from cartilage graded from 0 to 4 (ICRS grades 0 to 4) with standard deviations indicated by the shaded areas. b) Baseline-corrected Raman spectra in the fingerprint and high-wavenumber regions. The 1063 $cm^{-1}$ S-O stretching band assigned to the -$OSO_3$-/-$OSO_3$OH groups of sulphated GAGs (sGAGs) is highlighted by the shaded vertical bar. c) Example spectrum with mixed Gaussian−Lorentzian functions fitted to the 1063 $cm^{-1}$ sGAG band (red line), the phenylalanine ring breathing mode as an internal standard at 1003 $cm^{-1}$ (red line) and adjacent bands (grey lines). d) Dot plot showing 1063/1003 $cm^{-1}$ band area ratios versus lesion grade, with diamonds depicting group means. Statistically significant differences between lesion grades and the associated $p$ values are shown above the dots.

five is documented to cause distortions in spectral profiles and introduce artefacts [51]. Second, the validity of an internal spectroscopic calibration standard such as the phenylalanine 1003 $cm^{-1}$ band is questionable because of potential undefined changes to the profile of the band as a result of global molecular changes in cartilage with disease progression, age and tissue depth. Finally, in our averaged spectra, the O-H stretching intensity assigned to molecular $H_2O$ was shown to increase with lesion severity (Fig. 1b). This suggests that the overall hydration level of the sGAGs varies with lesion grade, which may have an unpredictable influence on the profile associated with the 1063 $cm^{-1}$ band [52]. Because of these considerations, we expanded our analyses of the Raman spectroscopy data to include assessment of the full wavenumber region including the high-wavenumber bands associated with O-H and C-H stretching vibrations.

### 3.2. *Examining spectral features across the full wavenumber range*

To better identify additional spectral changes occurring as a function of cartilage degeneration state, we attempted a multivariate data analysis approach in which spectral changes across the entire wavenumber range were considered. As a first multivariate data analysis approach, we analysed difference spectra obtained for the three sample groups (grades 1, 2/3 and 4) relative to the grade 0 control group (Fig. 2). Similar to the findings of the 1063 versus 1003 $cm^{-1}$ band ratio analysis, we observed an intensity increase in the 1063 $cm^{-1}$ S-O stretching band for the earliest lesion grade cartilage (grade 1) with respect to the control (Fig. 2a). Several other bands were also elevated in this region, and these increases were particularly marked for the bands above 1300 $cm^{-1}$. An elevation of the sGAG content and the contents of other protein constituents at this early lesion grade would suggest an increase in the synthesis or accumulation of some cartilage components, which might indicate a mechanism for the initial reparative processes occurring early in OA [53]. In response to tissue damage, chondrocytes appear to compensate by active proliferation and enhanced synthesis of matrix components including sGAGs [53–55]. We propose that failure of the reparative process causes a shift towards elevated catabolism, with cartilage destruction ensuing as evidenced by the large intensity reduction for multiple bands across the fingerprint region at more advanced lesion stages (Fig. 2b, c).

Interestingly, in addition to the changes in band intensities, we observed a broad fluorescence feature spanning 600–850 $cm^{-1}$ that increased in intensity with cartilage lesion grade (Fig. 2b, c, arrow). Biological materials inherently produce strong background fluorescence signals that can interfere with weaker Raman signals. Typically, fluorescence can be diminished or eliminated by the use of a 785 nm laser excitation source, as was the case in our work. However, because of the pattern of growth observed for the fluorescence signal with lesion progression, we concluded that this broad fluorescence was related to a specific aspect of the degeneration occurring in the cartilage specimens. Although we are not certain about the source of the fluorescence, we speculate that it may be related to advanced glycation end products (AGEs) [56,57], and the strength of fluorescence signals as a measure of general cartilage degradation has been recognised in an autofluorescence lifetime study [58].

In the high-wavenumber region, a similar trend was observed in cartilage of grade 1 and above in which a systematic decrease in the intensity of the CH stretching vibration band (2800–3000 $cm^{-1}$) was accompanied by enhanced intensity in the O-H stretching region (3000–3600 $cm^{-1}$) (Fig. 2d). These alterations correlate with the loss of tissue constituents and observed increase in water content (Table 1 and

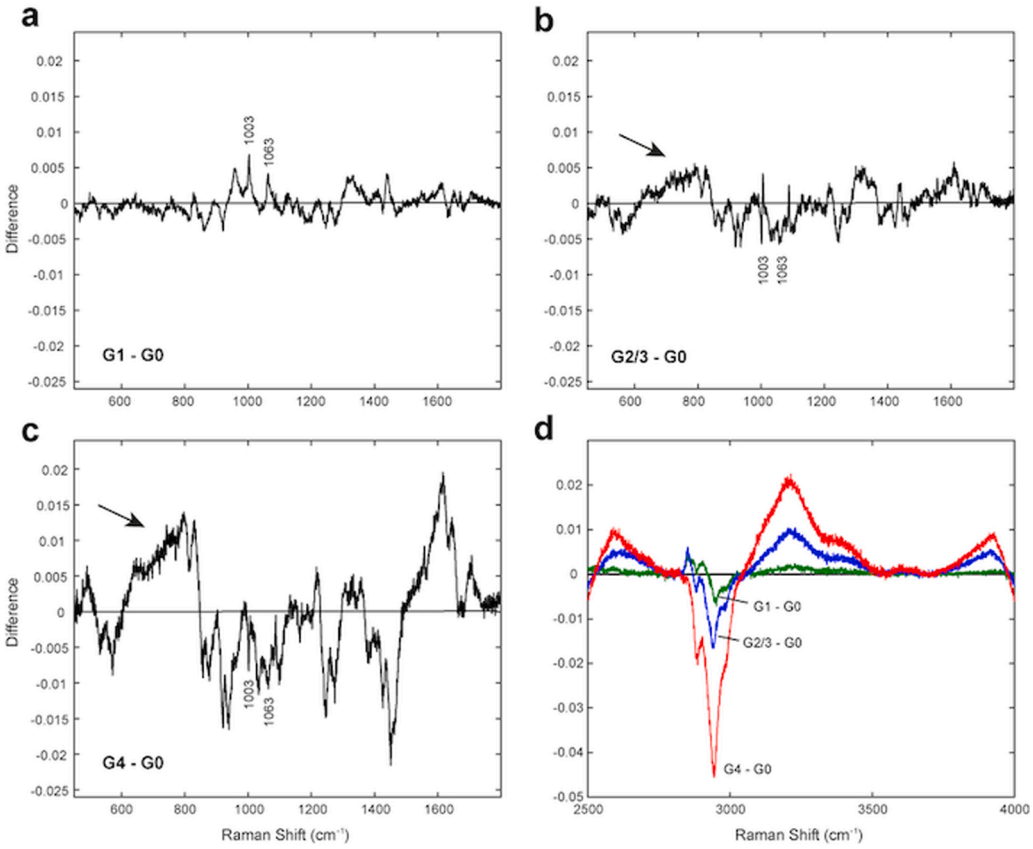


**Fig. 2.** Difference spectra in the fingerprint and high-wavenumber regions. Differences are shown between a) grade 1 and normal (grade 0) cartilage, b) grade 2/3 and normal cartilage, c) grade 4 and normal cartilage and d) each lesion grade and normal cartilage in the high-wavenumber region. The growth in intensity between grade 2/3 and grade 4 of a difference feature arising from increased fluorescence in the 600–850 $cm^{-1}$ range is indicated with arrows in b) and c).

Supplementary Fig. 1b), demonstrating an increase in cartilage hydration observed through the elevation of the O-H stretching band intensity. This is in agreement with the notion that the weakening of peptide bonds within the ECM, accompanied by the loss of sGAGs, results in structural disorganisation of the collagenous network. This loss of structural order is manifested by the breakdown of both the intra- and inter-molecular bonds in the helical part of collagen molecules, which can be correlated with observed increases in the total water content of OA cartilage [9,55].

By applying PCA to data acquired from the fingerprint region, we were able to distinguish only the more advanced (grade 4) cartilage from the other specimens (the healthy control and grades 0, 1 and 2/3) (Fig. 3a). The associated loading plot showed that the control and early lesion stages were characterised by the sGAG band at 1063 $cm^{-1}$ assigned to S-O stretching, a band at 1426 $cm^{-1}$ associated with the COO- vibration and a disulphide stretching band at 531 $cm^{-1}$ that probably originates from the disulphide bridges of ECM proteins (Fig. 3b). In addition, the control and early lesion cartilage featured several protein bands including those at 570 $cm^{-1}$ (tryptophan), 856 $cm^{-1}$ (C-C stretching, proline), 879 $cm^{-1}$ (C-C stretching, hydroxyproline), 920 $cm^{-1}$ (C-C stretching, proline ring), 939 $cm^{-1}$ (collagen, C-C stretching, proline in alpha helix), 1003 and 1033 $cm^{-1}$ (phenylalanine ring breathing vibrations), 1098 $cm^{-1}$ (C-N stretching, proteins), 1245 and 1270 $cm^{-1}$ (amide III bands and N-H bending vibrational modes) and 1451 $cm^{-1}$ (assigned to methylene deformation in biomolecules [34,38,59–61]). This suggests that the total biomaterial concentration, and in particular the protein content, is significantly higher in the control as well as at the early lesion stages compared to the grade 4 lesions (late-stage disease). This is consistent with the higher rate of catabolism associated with the later stages of cartilage disease and the concomitant loss of tissue components observed in the difference spectra in Fig. 2b, c.

By contrast, the spectra of the late-stage disease cartilage were dominated by water bands at 1622 and 1645 $cm^{-1}$. These bands are thought to be assigned to the H-O-H vibrations of partially hydrogen-bonded (three-bonded) and fully hydrogen-bonded (four-bonded) water [62,63], which are involved in the conformation and stabilisation of fibrillar collagen [64]. This suggests that the molecular water signatures may be associated with fibrillar collagen type II within the cartilage. Late-stage disease cartilage also featured strong bands centred at 489 and 800 $cm^{-1}$ for which the exact assignment is not yet clear, although it is possible that these bands originate from the molecular products of cartilage degradation. A prominent collagen band at 831 $cm^{-1}$ and a carbonyl vibration band at 1702 $cm^{-1}$ characteristic of proteins were also seen [61,65] (Fig. 3b).

The high-wavenumber region of the Raman spectrum is known to contain bands of lesser molecular specificity but higher signal intensity [65]. PCA of this region indicated that it was possible to discriminate the grade 0 control group from the earliest signs of pathology represented by the grade 1 specimens (Fig. 3c). The control group was characterised by bands at 2951 and 2995 $cm^{-1}$, which were tentatively assigned to $\nu(CH_3)$ modes of proteins, while the grade 1 lesions were characterised by bands at 2852, 2874 and 2917 $cm^{-1}$ tentatively assigned to $\nu(CH_2)$ and $\nu(CH_3)$ modes of lipids [65,61] (Fig. 3d). This result indicates that by examining the high-wavenumber region, it is possible to discriminate OA at significantly earlier stages in terms of changes in the vibrational signatures of methylene and methyl groups. Although the exact molecular origin of these differences is yet to be determined, this observation holds promise for clinical application following further development and

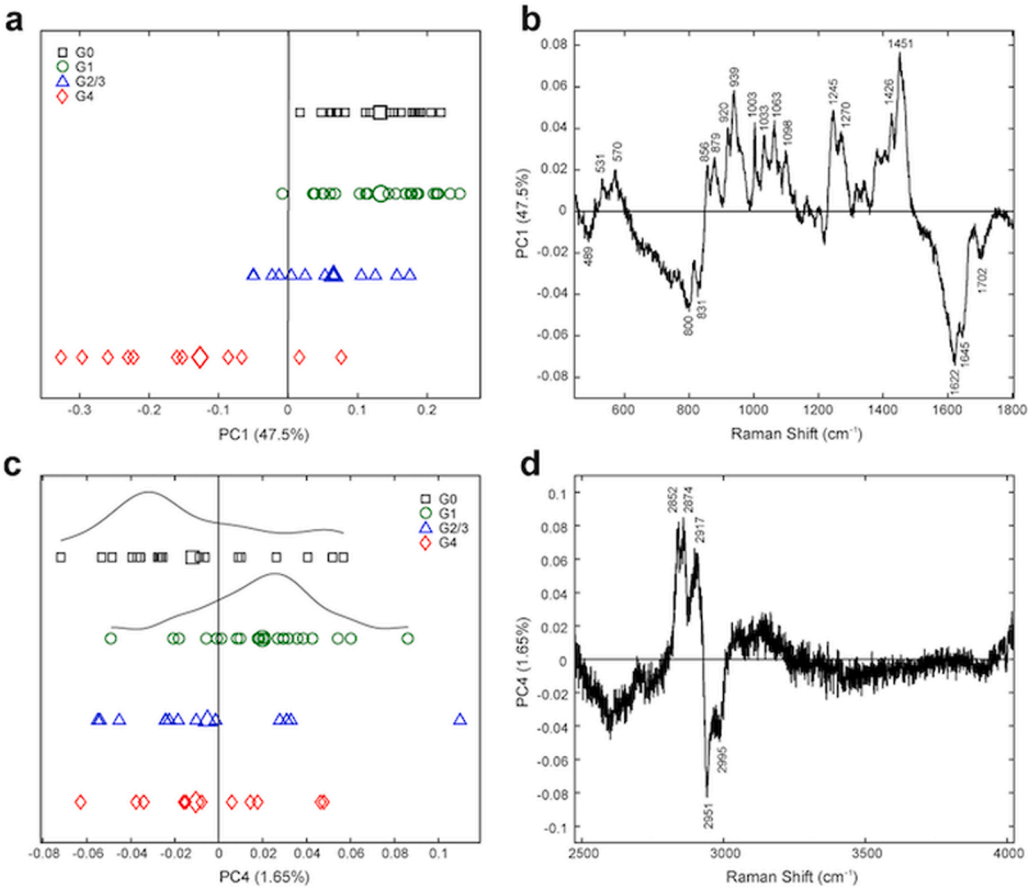


**Fig. 3.** Principal component analyses of the spectra in the fingerprint and high-wavenumber regions. a) One-dimensional PC1 score plot for the fingerprint region spectra of each lesion grade and b) corresponding PC1 loading plot. c) One-dimensional PC4 score plot for the high-wavenumber region spectra of each lesion grade and d) corresponding PC4 loading plot. In a) and c) the small symbols indicate individual spectra and the larger bold symbols show the spectral mean.

validation. A comprehensive list of tentatively assigned Raman bands can be found in Supplementary Table 3.

### 3.3. Raman spectroscopy of knee joint cartilage at arthroscopy

Having demonstrated the power of Raman spectroscopy to identify changes in cartilage composition that may be clinically meaningful, we investigated the potential to retrieve real-time Raman spectra in an in-clinic feasibility study, which is a first of its kind for knee joint arthroscopy to our knowledge. Prior to carrying out the in-clinic tests, the arthroscopic optical probe was trialled on cadaveric specimens (intact knees). It was determined that interpretable spectra could be obtained within 2 min, which might be acceptable in a clinical setting (data not shown).

In the theatre, the sterilised arthrospectroscopic probe was connected to the fibre-optic output of the spectrometer and positioned in the joint against the cartilage. This enabled single-point spectra to be acquired both from cartilage that appeared macroscopically normal and from obvious lesions at arthroscopy (Fig. 4 and Supplementary Fig. 3). These spectra, and in particular the prominent phenylalanine ring breathing vibrational band at 1003 $cm^{-1}$ (Fig. 4), demonstrate that it is possible to obtain Raman spectra with adequate signal-to-noise levels in a clinical setting.

Sulphate and phenylalanine band area ratios, $A_{1063}/A_{1003}$, were calculated for the spectra obtained from each patient to compare between apparently morphologically normal cartilage (N) and eroding cartilage (L). The $A_{1063}/A_{1003}$ ratio was found to be below 1 in the eroding cartilage in three patients (patients 1, 2 and 3, with $A_{1063}/A_{1003}$ ratios of 0.12, 0.44 and 0.63, respectively). From the *ex vivo* analysis, we know that these low $A_{1063}/A_{1003}$ ratios are most probably associated with the reduction in sGAG concentration in areas of cartilage erosion (Fig. 4a–c). Whist this was not an unexpected finding, it was interesting to note that this ratio was also observed to be reduced in cartilage that was apparently visually normal in patient 2 ($A_{1063}/A_{1003}$ ratio of 0.57, Fig. 4b) and patient 3 ($A_{1063}/A_{1003}$ ratio of 0.14, Fig. 4c). This is of significance because loss of proteoglycans prior to overt fibrillation of the cartilage surface has been established *in vivo* in models [66,67]. This suggests that *in vivo* disease-associated molecular changes extend into the cartilage immediately adjacent to the lesion margin that otherwise appears macroscopically normal and is deemed mechanically normal at arthroscopy. These subtle primary changes potentially could progress to full lesions [2] and result in the formation of larger lesions. Thus, the ability to identify such changes non-destructively would be a valuable tool to inform surgical decisions or interventions.

By contrast, patient 4 showed an elevation in the $A_{1063}/A_{1003}$ ratio at the lesion site compared to that at the macroscopically normal cartilage site (Fig. 4d). Although the reason for this is not clear, one possible explanation is that this spectrum was acquired from a region of lesion site cartilage that was undergoing an active reparative process in response to tissue damage, resulting in enhanced synthesis of matrix molecules [53]. Alternatively, this increased band ratio could have arisen because of a heterogeneous distribution of sGAGs throughout the cartilage, as reported by Williams et al. [23]. We acknowledge that the small number of patients tested in this study places limitations on the

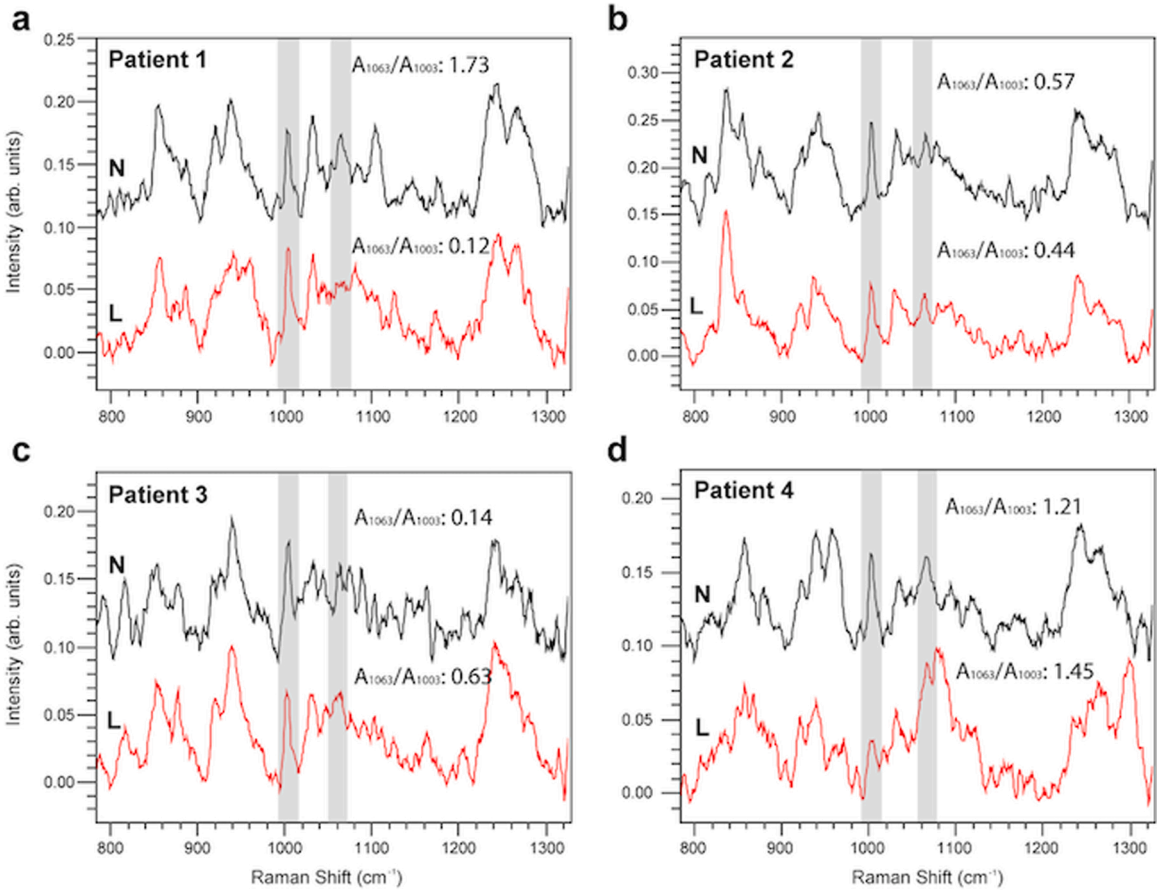


**Fig. 4.** Spectra obtained from in-clinic tests. Prior to collection of the Raman spectra under minimal room lighting, the optical probe was positioned against the femoral condyle cartilage surface within the knee of four patients, a)–d), respectively. Raman spectra collected from regions of cartilage that were visually normal but within 10–15 mm of eroding regions are shown in black (N). Raman spectra collected from areas of partial erosions (lesions) are shown in red (L). Shaded vertical panels highlight the ring breathing vibration of phenylalanine at 1003 $cm^{-1}$ and the $\nu_1$ vibrational mode of the sulphate -$OSO_3$- group at 1063 $cm^{-1}$. Area ratios for these two bands, $A_{1063}/A_{1003}$, were calculated and are shown alongside the respective spectra. Details of patient clinical features are given in Supplementary Table 2.

extrapolation of the data. However, the additional information gained from this proof-of-concept study highlights the insufficiency of using a single band ratio (such as the 1063 $cm^{-1}$/1003 $cm^{-1}$ ratio) for predictive or diagnostic classification. Thus, we emphasise the need to utilise a larger portion of the spectrum that encompasses a multitude of bands, as demonstrated by the superior classification achieved using the water bands in the high-wavenumber region (Fig. 3c). Because of the limited number of observations of Raman spectra from patient knees, we did not attempt to perform a multivariate evaluation. Nonetheless, these preliminary results are of significance as they demonstrate that Raman spectroscopy using optical spectroscopic probes compatible with established arthroscopic techniques can be implemented to play a useful role during orthopaedic surgery.

In the current work a linear optical probe design was used as this was

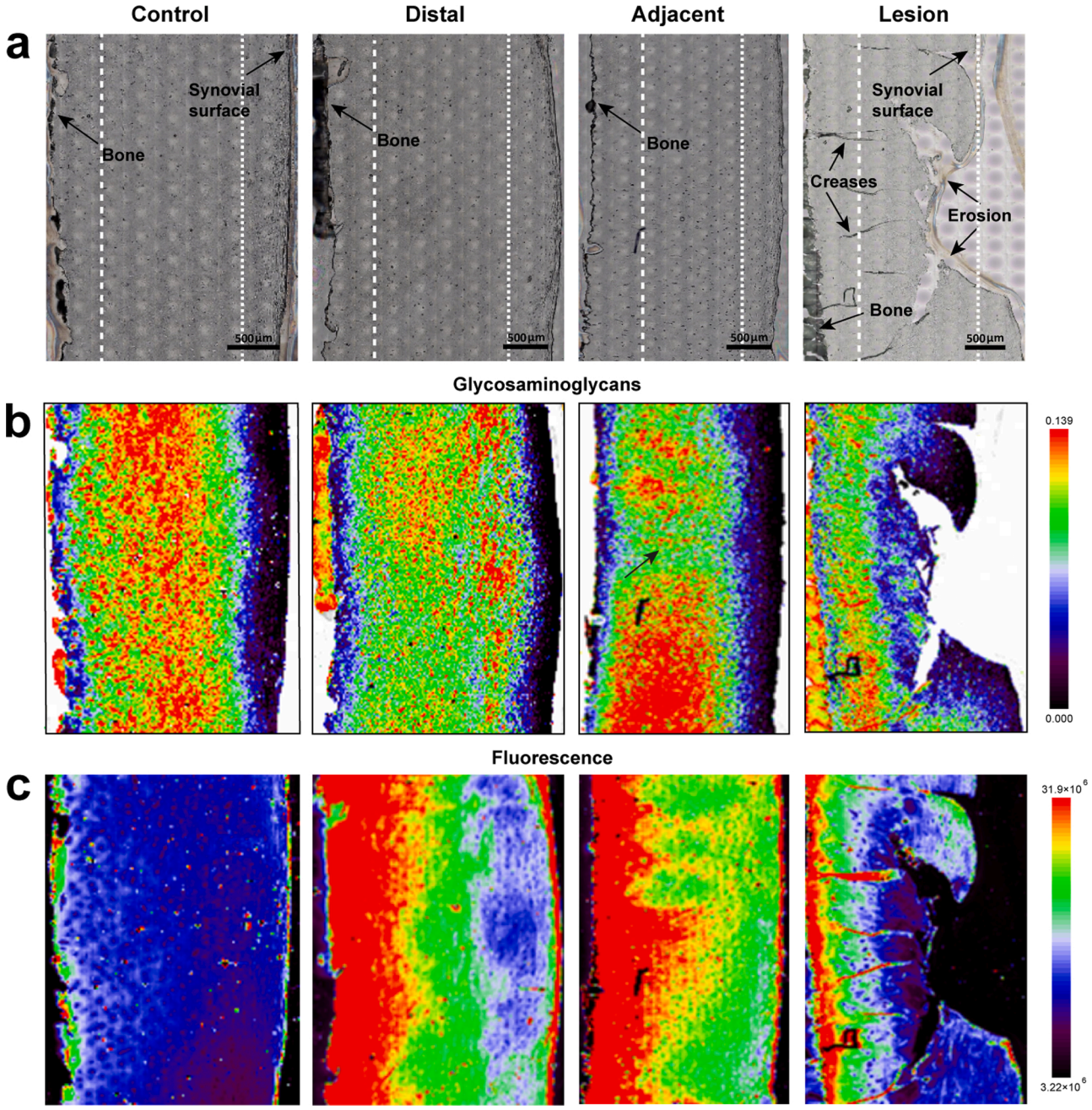


**Fig. 5.** Raman mapping study of cartilage. Raman maps were obtained from cartilage sections prepared in the sagittal plane (synovial surface to bone) to generate spectral maps of the full depth of the cartilage. A normal cartilage section (control) was prepared from the medial femoral condyle of an 18-year-old donor. Sections were also prepared from a joint containing a partial-thickness focal lesion in the medial femoral condyle (47-year-old donor). Additional sections were prepared from the same joint, from cartilage bordering the lesion (adjacent) that otherwise appeared macroscopically normal and from a more distal site on the femoral condyle that was used as an intra-joint control (see Supplementary Fig. 1 for details of sampling sites). a) Brightfield images of unstained sections of distal, adjacent and lesion site cartilage and control (normal) cartilage. Regions of residual bone, erosion and small creases (tissue folds generated in the lesion site sample during histological mounting) are labelled. The vertical dashed white lines mark the approximate zones commonly used to denote organisation of the cartilage (synovial zone, transition or mid-zone and deep or calcified zone). b) DCLS analysis of the distribution of sGAGs across the same cartilage sections illustrating the marked differences in distribution between the normal (control) cartilage and the apparently normal cartilage sites in the joint with the lesion. c) Fluorescence distributions across the cartilage sections shown in a). The fluorescence signals were obtained from the areas subtracted from the raw Raman spectra during baseline correction. The folds in the cartilage appear as highly fluorescent artefacts that project beyond the boundary of the deep zone.

the ideal shape to probe the femoral condyle at knee flexion. However, further development of the optical probes should include the incorporation of design features tuned to the topography of the cartilage surface within the joint to enable the acquisition of spectra from distal or proximal regions of the condyles and the trochlear groove. It may be possible to develop probes based on fibre optics to deliver a laser beam and collect Raman photons within the hooked end of an arthroscopic probe. The main challenges are to enhance the collection efficiency of the probe for the rapid acquisition of spectra that span a wide range of Raman shifts and map a wider area. The development of fibre arrays, adaptive-focus optical fibre tips and fibre tip fabrication may overcome some of these challenges [68–72].

### 3.4. Raman mapping studies of cartilage

Our initial studies revealed the limitations of point spectra for cartilage assessment. Further problems arise with this approach because of the anisotropic biomolecular composition of cartilage; variations in content are known to occur through its depth from the synovial surface to the subchondral bone [6,73]. The thinning of cartilage, observed with age and OA, further undermines the value of point measurements in evaluating disease-related changes. For example, changes in the proportion of collagen to proteoglycans may influence the absolute intensity of the phenylalanine ring breathing vibration at 1003 $cm^{-1}$, as this residue is present in different amounts in the two protein components. In addition, we have observed changes in the intensity, Raman shift and width of the S-O stretching band as a function of tissue degradation (Fig. 1). These confounding factors need careful consideration to properly evaluate the issues that might affect the interpretation of articular cartilage spectra. We therefore conducted Raman mapping of the axial plane of cartilage specimens (synovial surface to subchondral bone) to track the spatial localisation and relative abundance of sGAGs across the margins of lesion sites (Fig. 5a).

To assess the relative abundance and distribution of sGAGs, we used a DCLS analysis with input reference Raman spectra for the main cartilage constituents to compare the Raman maps of the control and lesion sites (Fig. 5b). sGAGs in the healthy control cartilage were predominantly localised in the middle-to-deep zone, with a uniform spatial distribution (Fig. 5b, *control*). The heat maps indicate that compared to the control, in cartilage that was distal to a lesion site that had a macroscopically normal appearance, the sGAG distribution was less uniform and the concentrations lower (Fig. 5b, *distal*). However, in cartilage adjacent to the lesion, the sGAG distribution was even more heterogeneous, with localised regions of reduced or elevated sGAG concentration (Fig. 5b, *adjacent*). Within the lesion, where the structural integrity of the cartilage was compromised, the sGAG concentration was higher in the deeper zone than in the superficial zone, where the heat map showed the lowest concentrations (Fig. 5b, *lesion*). The varying levels of sGAG within the cartilage zones and between cartilage sites may be indicative of localised regions with varying degrees of proteoglycan loss or biosynthetic activity. Although mechanisms for both proteoglycan loss and biosynthetic activity have been shown to operate in cartilage disease models using biochemical assay methods, the submillimetre spatial resolution of our Raman maps provides a more detailed picture of the underlying molecular alterations within lesions and in the apparently healthy adjacent cartilage. Furthermore, the focal loss of sGAG observed in the cartilage adjacent to the margin of a lesion supports the findings of our in-clinic study in which a decrease in sGAGs was observed in macroscopically normal cartilage adjacent to lesions.

The Raman mapping studies provided a better insight into the cartilage fluorescence observed in the difference spectra in the previous analysis. The control sample exhibited the lowest fluorescence intensities across all cartilage zones (Fig. 5c, *control*), compared to the corresponding zones in the macroscopically normal cartilage sampled from sites adjacent and distal to the lesion site. (Fig. 5c, *adjacent* and *distal*). The fluorescence emission signal was more intense in the superficial zone in both the adjacent and distal cartilage, and among these two specimens, the increase was more gradual for the cartilage proximal to the lesion. We speculate that these differences in spectra between normal cartilage and cartilage that is of normal appearance but from a joint with a small lesion suggest that the lesion influences the joint milieu across the whole joint to induce metabolic changes. Furthermore, the fluorescence intensity was diminished at the surface of the residual cartilage in the lesion (fibrillated cartilage) compared to that in the deep zone below the lesion (Fig. 5c, *lesion*). The greater level of detail on fluorescence localisation across a large region of cartilage provided by this type of mapping study could lead to a better understanding of the dynamic metabolic changes governing cartilage components such as AGEs. Cartilage accumulates AGEs, which are fluorescent derivatives arising from non-enzymatic modification of amino groups by non-reducing sugars [57,56]. Cartilage collagen, which has a half-life of over 100 years, is prone to AGE accumulation due to its slow turnover [74]; hence, it is plausible that the lower fluorescence intensity within the fibrillating site may be associated with collagen loss by proteolytic action and faster tissue remodelling compared to normal (healthy) cartilage. The half-life of aggrecan is shorter, having been measured in cartilage as 3.4 years, although degradation products from its amino-terminus region can accumulate with age in smaller amounts [7] and exhibit a half-life of 25 years [75]. Consequently, its contribution to AGE-related fluorescence may be less prominent than that of collagen.

The mapping results demonstrate that substantial differences exist between healthy young cartilage and macroscopically normal cartilage from a joint with a spontaneous local lesion. This warrants further investigation. Specifically, whether joints with more advanced lesions have distinct biochemical differences in the unaffected cartilage should be definitively established. A natural extension to this work would be to investigate the age-related biochemical differences in cartilage from young and old donors without lesions, to establish a baseline that will further substantiate the suitability of the use of various control cartilage specimens. Nevertheless, the observed differences in the concentrations and distributions of sGAGs indicate that Raman mapping studies of cartilage are not only essential for the assessment of specific molecular constituent distributions through its zonal structure, but also offer the potential to quantify concentrations and understand the significance for cartilage health of the biochemical alterations. The current Raman mapping technique is limited to *ex vivo* analysis of cartilage specimens but has the potential to be developed further to inform *in vivo* studies in which Raman-based optical probes are to be utilised. It would also be an invaluable imaging system for quality and process control in tissue engineering strategies, facilitating the live monitoring of product quality.

The Raman mapping study produced superior topographical detail across a wide area of cartilage that would have been impossible to obtain with commonly used single-point approaches. This is of significance because of the anisotropic nature of cartilage, where pathology-related molecular alterations need to be carefully distinguished from normal spatial variations in tissue biochemistry.

## 4. Conclusion

Our study extends earlier work and increases the certainty that clinically relevant changes in molecular species that precede macroscopic cartilage degeneration are detectable by Raman spectroscopy in the fingerprint wavenumber region. More specifically, in this work we established that it is possible to assess quantitatively the loss of -$OSO_3$- groups from sGAGs together with changes in tissue hydration in cartilage containing small focal lesions. In addition, changes in multiple bands across the fingerprint region can provide a more comprehensive analysis of biosynthetic and catabolic processes in more advanced disease stages It is noteworthy that fingerprint-region Raman spectra can be recorded in joints of patients. This result is of significant value in highlighting the potential for further development of Raman techniques

for clinical use. The ability to record clinically useful Raman maps with sub-millimetre resolution *in vivo* has important implications for the topographical assessment of cartilage health across the joint, particularly with respect to therapeutic options and disease progression. Furthermore, validation of this technique is necessary for its successful integration into clinical practice and could proceed by exploring the impact of several different experimental parameters such as variations in signal output at different depths of probing. It will also be of interest to explore the value of methyl and methylene C-H stretch Raman signals in the high-wavenumber region, as we have shown that these vibrational bands can allow better discrimination of samples with earlier compositional changes.

## Funding

ADGN was supported by a grant from the National Institute for Health Research [i4i II-FS-0909-13007]. RG was supported by Versus Arthritis UK and the Medical Technologies Innovation and Knowledge Centre [grant 21159], and by an Engineering and Physical Sciences Research Council Impact Acceleration Account2017-20 Discovery-To-Use (D2U) award administered by University College London Innovation and Enterprise office. Additional support was provided by the London Development Agency (Heptagon fund) and RVC Business department, Knowledge Transfer and Impact.

## Author contributions

JD, ERCD and PFM conceived the study and carried out and interpreted the initial series of Raman experiments. JD, PFM and ADGN designed and tested the *in vivo* Raman probe that was implemented by RS with the assistance of JD and ADGN during pioneering surgical experiments. RG re-interpreted the original datasets using statistical analysis techniques with NB. RG and GMHT carried out and interpreted the Raman mapping of tissue samples. JD, RG and PFM wrote the main draft of the manuscript, which was commented on and edited by all the authors.

## Ethics approval

The study was approved by the Royal Veterinary College Ethics and Welfare Committee (Approval URN 2010 0004H and 2016 1467) and Imperial College NHS Trust Research Ethics Committee (10/H0711/2).

## Consent to participate

All patients signed a written informed consent form to participate in the study.

## Declaration of Competing Interest

The authors report no declarations of interest.

## Availability of data and material

The datasets generated during the current study are deposited on institutional servers for further analyses and data mining but are available from the corresponding author on reasonable request.

## Acknowledgements

We would like to thank Renishaw plc (Wotton-under-Edge, Gloucester, UK) for the use of a RA816 Biological Analyser for the Raman mapping studies. We also acknowledge Dr Orlagh Carroll for help with biostatistics and Dr Ian Bell for help with navigating the WiRE software. The Royal Veterinary College manuscript approval number is 1547874.

## Appendix A. Supplementary data

Supplementary material related to this article can be found, in the online version, at https://doi.org/10.1016/j.clispe.2021.100012.

## References

[1] E.B. Hunziker, A. Stahli, Surgical suturing of articular cartilage induces osteoarthritis-like changes, Osteoarthritis Cartilage. 16 (9) (2008) 1067–1073, https://doi.org/10.1016/j.joca.2008.01.009.
[2] T.M. Simon, H.M. Aberman, Cartilage regeneration and repair testing in a surrogate large animal model, Tissue Eng Part B Rev. 16 (1) (2010) 65–79, https://doi.org/10.1089/ten.TEB.2009.0304.
[3] H. Madry, F.P. Luyten, A. Facchini, Biological aspects of early osteoarthritis, Knee Surg Sports Traumatol Arthrosc. 20 (3) (2012) 407–422, https://doi.org/10.1007/s00167-011-1705-8.
[4] H.A. Wieland, M. Michaelis, B.J. Kirschbaum, K.A. Rudolphi, Osteoarthritis - an untreatable disease? Nat Rev Drug Discov. 4 (4) (2005) 331–344, https://doi.org/10.1038/nrd1693.
[5] M. Cross, E. Smith, D. Hoy, S. Nolte, I. Ackerman, M. Fransen, et al., The global burden of hip and knee osteoarthritis: estimates from the global burden of disease 2010 study, Ann Rheum Dis. 73 (7) (2014) 1323–1330, https://doi.org/10.1136/annrheumdis-2013-204763.
[6] C. Muller, A. Khabut, J. Dudhia, F.P. Reinholt, A. Aspberg, D. Heinegard, et al., Quantitative proteomics at different depths in human articular cartilage reveals unique patterns of protein distribution, Matrix Biol. 40 (2014) 34–45, https://doi.org/10.1016/j.matbio.2014.08.013.
[7] J. Dudhia, Aggrecan, aging and assembly in articular cartilage, Cell Mol Life Sci. 62 (19-20) (2005) 2241–2256, https://doi.org/10.1007/s00018-005-5217-x.
[8] A. Maroudas, M.T. Bayliss, M.F. Venn, Further studies on the composition of human femoral head cartilage, Ann Rheum Dis. 39 (5) (1980) 514–523, https://doi.org/10.1136/ard.39.5.514.
[9] A. Maroudas, M. Venn, Chemical composition and swelling of normal and osteoarthrotic femoral head cartilage. II. Swelling, Ann Rheum Dis. 36 (5) (1977) 399–406, https://doi.org/10.1136/ard.36.5.399.
[10] W. Wu, R.C. Billinghurst, I. Pidoux, J. Antoniou, D. Zukor, M. Tanzer, et al., Sites of collagenase cleavage and denaturation of type II collagen in aging and osteoarthritic articular cartilage and their relationship to the distribution of matrix metalloproteinase 1 and matrix metalloproteinase 13, Arthritis Rheum. 46 (8) (2002) 2087–2094, https://doi.org/10.1002/art.10428.
[11] J.R. Matyas, L. Atley, M. Ionescu, D.R. Eyre, A.R. Poole, Analysis of cartilage biomarkers in the early phases of canine experimental osteoarthritis, Arthritis Rheum. 50 (2) (2004) 543–552, https://doi.org/10.1002/art.20027.
[12] C. McDevitt, E. Gilbertson, H. Muir, An experimental model of osteoarthritis; early morphological and biochemical changes, J Bone Joint Surg Br. 59 (1) (1977) 24–35, https://doi.org/10.1302/0301-620X.59B1.576611.
[13] D.M. Visco, B. Johnstone, M.A. Hill, G.A. Jolly, B. Caterson, Immunohistochemical analysis of 3-B-(-) and 7-D-4 epitope expression in canine osteoarthritis, Arthritis Rheum. 36 (12) (1993) 1718–1725, https://doi.org/10.1002/art.1780361211.
[14] F. Nelson, R.C. Billinghurst, I. Pidoux, A. Reiner, M. Langworthy, M. McDermott, et al., Early post-traumatic osteoarthritis-like changes in human articular cartilage following rupture of the anterior cruciate ligament, Osteoarthritis Cartilage. 14 (2) (2006) 114–119, https://doi.org/10.1016/j.joca.2005.08.005.
[15] P.J. Roughley, J.S. Mort, The role of aggrecan in normal and osteoarthritic cartilage, J Exp Orthop. 1 (1) (2014) 8, https://doi.org/10.1186/s40634-014-0008-7.
[16] D.P. Page Thomas, B. King, T. Stephens, J.T. Dingle, In vivo studies of cartilage regeneration after damage induced by catabolin/interleukin-1, Ann Rheum Dis. 50 (2) (1991) 75–80, https://doi.org/10.1136/ard.50.2.75.
[17] A. Williams, R.A. Oppenheimer, M.L. Gray, D. Burstein, Differential recovery of glycosaminoglycan after IL-1-induced degradation of bovine articular cartilage depends on degree of degradation, Arthritis Res Ther. 5 (2) (2003) R97–105, https://doi.org/10.1186/ar615.
[18] P.S. Emrani, J.N. Katz, C.L. Kessler, W.M. Reichmann, E.A. Wright, T.E. McAlindon, et al., Joint space narrowing and Kellgren-Lawrence progression in knee osteoarthritis: an analytic literature synthesis, Osteoarthritis Cartilage. 16 (8) (2008) 873–882, https://doi.org/10.1016/j.joca.2007.12.004.
[19] E. Calvo, I. Palacios, E. Delgado, J. Ruiz-Cabello, P. Hernandez, O. Sanchez-Pernaute, et al., High-resolution MRI detects cartilage swelling at the early stages of experimental osteoarthritis, Osteoarthritis Cartilage. 9 (5) (2001) 463–472, https://doi.org/10.1053/joca.2001.0413.
[20] W. Li, R. Scheidegger, Y. Wu, R.R. Edelman, M. Farley, N. Krishnan, et al., Delayed contrast-enhanced MRI of cartilage: comparison of nonionic and ionic contrast agents, Magn Reson Med. 64 (5) (2010) 1267–1273, https://doi.org/10.1002/mrm.22555.
[21] W. Ling, R.R. Regatte, G. Navon, A. Jerschow, Assessment of glycosaminoglycan concentration in vivo by chemical exchange-dependent saturation transfer (gagCEST), Proc Natl Acad Sci U S A. 105 (7) (2008) 2266–2270, https://doi.org/10.1073/pnas.0707666105.
[22] H. Owman, C.J. Tiderius, P. Neuman, F. Nyquist, L.E. Dahlberg, Association between findings on delayed gadolinium-enhanced magnetic resonance imaging of cartilage and future knee osteoarthritis, Arthritis Rheum. 58 (6) (2008) 1727–1730, https://doi.org/10.1002/art.23459.

[23] A. Williams, A. Gillis, C. McKenzie, B. Po, L. Sharma, L. Micheli, et al., Glycosaminoglycan distribution in cartilage as determined by delayed gadolinium-enhanced MRI of cartilage (dGEMRIC): potential clinical applications, AJR Am J Roentgenol. 182 (1) (2004) 167–172, https://doi.org/10.2214/ajr.182.1.1820167.

[24] S. Nebelung, M. Post, M. Knobe, M. Tingart, P. Emans, J. Thuring, et al., Detection of Early-Stage Degeneration in Human Articular Cartilage by Multiparametric MR Imaging Mapping of Tissue Functionality, Sci Rep. 9 (1) (2019) 5895, https://doi.org/10.1038/s41598-019-42543-w.

[25] L.L. Laslett, J.-P. Pelletier, F.M. Cicuttini, G. Jones, J.-P. Martel-Pelletier, Measuring Disease Progression in Osteoarthritis, Current Treatment Options in Rheumatology. 2 (2) (2016) 97–110, https://doi.org/10.1007/s40674-016-0041-z.

[26] U. Ahmed, A. Anwar, R.S. Savage, M.L. Costa, N. Mackay, A. Filer, et al., Biomarkers of early stage osteoarthritis, rheumatoid arthritis and musculoskeletal health, Sci Rep. 5 (2015) 9259, https://doi.org/10.1038/srep09259.

[27] J.B. Catterall, T.V. Stabler, C.R. Flannery, V.B. Kraus, Changes in serum and synovial fluid biomarkers after acute injury (NCT00332254), Arthritis Res Ther. 12 (6) (2010) R229, https://doi.org/10.1186/ar3216.

[28] C.R. Chu, A.A. Williams, C.H. Coyle, M.E. Bowers, Early diagnosis to enable early treatment of pre-osteoarthritis, Arthritis Res Ther. 14 (3) (2012) 212, https://doi.org/10.1186/ar3845.

[29] R. Kumar, A. Kumar, Assessment of Articular Cartilage by Second Harmonic Microscopy: Challenges and Opportunities, Frontiers in Physics. 7 (137) (2019), https://doi.org/10.3389/fphy.2019.00137.

[30] Krishnan Y, Grodzinsky AJ, Cartilage diseases. Matrix Biol. 71-72 (2018) 51–69, https://doi.org/10.1016/j.matbio.2018.05.005.

[31] J.K. Sarin, N.C.R. Te Moller, I.A.D. Mancini, H. Brommer, J. Visser, J. Malda, et al., Arthroscopic near infrared spectroscopy enables simultaneous quantitative evaluation of articular cartilage and subchondral bone in vivo, Sci Rep. 8 (1) (2018) 13409, https://doi.org/10.1038/s41598-018-31670-5.

[32] E.R.C. Draper, J. Dudhia, P.F. McMillan, S. Firth, inventor Tissue assessment, 2008.

[33] J. Dudhia, P.F. McMillan, E.R.C. Draper, S. Firth, Imaging early molecular alterations in articular cartilage degeneration by Raman spectroscopy, Int J Exp Pathol. (2009) A32–A33.

[34] K.A. Esmonde-White, F.W. Esmonde-White, M.D. Morris, B.J. Roessler, Fiber-optic Raman spectroscopy of joint tissues, Analyst. 136 (8) (2011) 1675–1685, https://doi.org/10.1039/c0an00824a.

[35] R. Kumar, K.M. Gronhaug, N.K. Afseth, V. Isaksen, C. de Lange Davies, J. O. Drogset, et al., Optical investigation of osteoarthritic human cartilage (ICRS grade) by confocal Raman spectroscopy: a pilot study, Anal Bioanal Chem. 407 (26) (2015) 8067–8077, https://doi.org/10.1007/s00216-015-8979-5.

[36] M.B. Albro, M.S. Bergholt, J.P. St-Pierre, A. Vinals Guitart, H.M. Zlotnick, E. G. Evita, et al., Raman spectroscopic imaging for quantification of depth-dependent and local heterogeneities in native and engineered cartilage, NPJ Regen Med. 3 (2018) 3, https://doi.org/10.1038/s41536-018-0042-7.

[37] M. Pudlas, E. Brauchle, T.J. Klein, D.W. Hutmacher, K. Schenke-Layland, Non-invasive identification of proteoglycans and chondrocyte differentiation state by Raman microspectroscopy, J Biophotonics. 6 (2) (2013) 205–211, https://doi.org/10.1002/jbio.201200064.

[38] E. Pavlou, X. Zhang, J. Wang, N. Kourkoumelis, Raman spectroscopy for the assessment of osteoarthritis, Annals of Joint. (2018) 3.

[39] A.D. Nunn, R.K. Strachan, S. Firth, E.R.C. Draper, P.F. McMillan, J. Dudhia, Intra-operative mapping of articular cartilage degeneration with Raman arthrospectroscopy, Int J Exp Pathol. 94 (2013) A19–A20.

[40] P. Lorenzo, M.T. Bayliss, D. Heinegard, Altered patterns and synthesis of extracellular matrix macromolecules in early osteoarthritis, Matrix Biol. 23 (6) (2004) 381–391, https://doi.org/10.1016/j.matbio.2004.07.007.

[41] R. Gaifulina, D.J. Caruana, D. Oukrif, N.J. Guppy, S. Culley, R. Brown, et al., Rapid and complete paraffin removal from human tissue sections delivers enhanced Raman spectroscopic and histopathological analysis, Analyst. 145 (4) (2020) 1499–1510, https://doi.org/10.1039/c9an01030k.

[42] A.T. Lewis, R. Gaifulina, M. Isabelle, J. Dorney, M.L. Woods, G.R. Lloyd, et al., Mirrored stainless steel substrate provides improved signal for Raman spectroscopy of tissue and cells, J Raman Spectrosc. 48 (1) (2017) 119–125, https://doi.org/10.1002/jrs.4980.

[43] R.W. Farndale, D.J. Buttle, A.J. Barrett, Improved quantitation and discrimination of sulphated glycosaminoglycans by use of dimethylmethylene blue, Biochim Biophys Acta. 883 (2) (1986) 173–177, https://doi.org/10.1016/0304-4165(86)90306-5.

[44] M. Fields, N. Spencer, J. Dudhia, P.F. McMillan, Structural changes in cartilage and collagen studied by high temperature Raman spectroscopy, Biopolymers. 107 (6) (2017), https://doi.org/10.1002/bip.23017.

[45] C. Slattery, C.Y. Kweon, Classifications in Brief: Outerbridge Classification of Chondral Lesions, Clin Orthop Relat Res. 476 (10) (2018) 2101–2104, https://doi.org/10.1007/s11999.0000000000000255.

[46] A. Cao, A.K. Pandya, G.K. Serhatkulu, R.E. Weber, H. Dai, J.S. Thakur, et al., A robust method for automated background subtraction of tissue fluorescence, Journal of Raman Spectroscopy. 38 (9) (2007) 1199–1205, https://doi.org/10.1002/jrs.1753.

[47] J. Trevisan, P.P. Angelov, A.D. Scott, P.L. Carmichael, F.L. Martin, IRootLab: a free and open-source MATLAB toolbox for vibrational biospectroscopy data analysis, Bioinformatics 29 (8) (2013) 1095–1097, https://doi.org/10.1093/bioinformatics/btt084.

[48] D. Uy, A.E. O'Neill, Principal component analysis of Raman spectra from phosphorus-poisoned automotive exhaust-gas catalysts, Journal of Raman Spectroscopy. 36 (10) (2005) 988–995, https://doi.org/10.1002/jrs.1395.

[49] N.K. Afseth, V.H. Segtnan, J.P. Wold, Raman spectra of biological samples: A study of preprocessing methods, Appl Spectrosc. 60 (12) (2006) 1358–1367, https://doi.org/10.1366/000370206779321454.

[50] K.H. Liland, A. Kohler, N.K. Afseth, Model-based pre-processing in Raman spectroscopy of biological samples, Journal of Raman Spectroscopy. 47 (6) (2016) 643–650, https://doi.org/10.1002/jrs.4886.

[51] J. Ferraro, K. Nakamoto, C. Brown, Introductory Raman Spectroscopy, 2 ed., Academic Press, Burlington, MA, 2003.

[52] M. Fields, Characterisation of articular cartilage by micro-beam Raman spectroscopy, UCL (University College London), Great Britain, 2016.

[53] M.K. Lotz, S. Otsuki, S.P. Grogan, R. Sah, R. Terkeltaub, D. D'Lima, Cartilage cell clusters, Arthritis Rheum. 62 (8) (2010) 2206–2218, https://doi.org/10.1002/art.27528.

[54] J.B. Kouri, S.A. Jimenez, M. Quintero, A. Chico, Ultrastructural study of chondrocytes from fibrillated and non-fibrillated human osteoarthritic cartilage, Osteoarthritis Cartilage. 4 (2) (1996) 111–125, https://doi.org/10.1016/s1063-4584(05)80320-6.

[55] Y. Henrotin, J.Y. Reginster, Anabolic events in osteoarthritis, Osteoarthritis Cartilage. 7 (3) (1999) 310–312, https://doi.org/10.1053/joca.1998.0175.

[56] N. Verzijl, J. DeGroot, R.A. Bank, M.T. Bayliss, J.W. Bijlsma, F.P. Lafeber, et al., Age-related accumulation of the advanced glycation endproduct pentosidine in human articular cartilage aggrecan: the use of pentosidine levels as a quantitative measure of protein turnover, Matrix Biol. 20 (7) (2001) 409–417, https://doi.org/10.1016/s0945-053x(01)00158-5.

[57] N. Verzijl, J. DeGroot, E. Oldehinkel, R.A. Bank, S.R. Thorpe, J.W. Baynes, et al., Age-related accumulation of Maillard reaction products in human articular cartilage collagen, Biochem J. 350 (Pt 2) (2000) 381–387.

[58] H.B. Manning, M.B. Nickdel, K. Yamamoto, J.L. Lagarto, D.J. Kelly, C.B. Talbot, et al., Detection of cartilage matrix degradation by autofluorescence lifetime, Matrix Biol. 32 (1) (2013) 32–38, https://doi.org/10.1016/j.matbio.2012.11.012.

[59] A. Bonifacio, C. Beleites, F. Vittur, E. Marsich, S. Semeraro, S. Paoletti, et al., Chemical imaging of articular cartilage sections with Raman mapping, employing uni- and multi-variate methods for data analysis, Analyst. 135 (12) (2010) 3193–3204, https://doi.org/10.1039/c0an00459f.

[60] J.C. Mansfield, C.P. Winlove, Lipid distribution, composition and uptake in bovine articular cartilage studied using Raman micro-spectrometry and confocal microscopy, J Anat. 231 (1) (2017) 156–166, https://doi.org/10.1111/joa.12624.

[61] Z. Movasaghi, S. Rehman, I.U. Rehman, Raman Spectroscopy of Biological Tissues, Applied Spectroscopy Reviews. 42 (5) (2007) 493–541, https://doi.org/10.1080/05704920701551530.

[62] G.E. Walrafen, L.A. Blatz, Weak Raman bands from water, The Journal of Chemical Physics. 59 (5) (1973) 2646–2650, https://doi.org/10.1063/1.1680382.

[63] D.M. Carey, G.M. Korenowski, Measurement of the Raman spectrum of liquid water, The Journal of Chemical Physics. 108 (7) (1998) 2669–2675, https://doi.org/10.1063/1.475659.

[64] J. Bella, B. Brodsky, H.M. Berman, Hydration structure of a collagen peptide, Structure. 3 (9) (1995) 893–906, https://doi.org/10.1016/S0969-2126(01)00224-6.

[65] M.S. Bergholt, A. Serio, M.B. Albro, Raman Spectroscopy: Guiding Light for the Extracellular Matrix, Front Bioeng Biotechnol. 7 (2019) 303, https://doi.org/10.3389/fbioe.2019.00303.

[66] M.F. Rai, R.H. Brophy, L.J. Sandell, Osteoarthritis following meniscus and ligament injury: insights from translational studies and animal models, Curr Opin Rheumatol. 31 (1) (2019) 70–79, https://doi.org/10.1097/BOR.0000000000000566.

[67] G.E. Narez, K.M. Fischenich, T.L.H. Donahue, Experimental animal models of post-traumatic osteoarthritis of the knee, Orthop Rev (Pavia). 12 (2) (2020) 8448, https://doi.org/10.4081/or.2020.8448.

[68] M.V. Schulmerich, W.F. Finney, R.A. Fredricks, M.D. Morris, Subsurface Raman spectroscopy and mapping using a globally illuminated non-confocal fiber-optic array probe in the presence of Raman photon migration, Appl Spectrosc. 60 (2) (2006) 109–114, https://doi.org/10.1366/000370206776023340.

[69] G. Kostovski, P.R. Stoddart, A. Mitchell, The optical fiber tip: an inherently light-coupled microscopic platform for micro- and nanotechnologies, Adv Mater. 26 (23) (2014) 3798–3820, https://doi.org/10.1002/adma.201304605.

[70] W. Yang, F. Knorr, J. Popp, I.W. Schie, Development and evaluation of a hand-held fiber-optic Raman probe with an integrated autofocus unit, Opt Express. 28 (21) (2020) 30760–30770, https://doi.org/10.1364/oe.401207.

[71] J.T. Motz, M. Hunter, L.H. Galindo, J.A. Gardecki, J.R. Kramer, R.R. Dasari, et al., Optical fiber probe for biomedical Raman spectroscopy, Appl Opt. 43 (3) (2004) 542–554, https://doi.org/10.1364/ao.43.000542.

[72] F. Nicolson, M.F. Kircher, N. Stone, P. Matousek, Spatially offset Raman spectroscopy for biomedical applications, Chem Soc Rev. 50 (1) (2021) 556–568, https://doi.org/10.1039/d0cs00855a.

[73] M.F. Hsueh, P. Onnerfjord, V.B. Kraus, Biomarkers and proteomic analysis of osteoarthritis, Matrix Biol. 39 (2014) 56–66, https://doi.org/10.1016/j.matbio.2014.08.012.

[74] D.R. Eyre, M.A. Weis, J.J. Wu, Articular cartilage collagen: an irreplaceable framework? Eur Cell Mater. 12 (2006) 57–63, https://doi.org/10.22203/ecm.v012a07.

[75] A. Maroudas, M.T. Bayliss, N. Uchitel-Kaushansky, R. Schneiderman, E. Gilav, Aggrecan turnover in human articular cartilage: use of aspartic acid racemization as a marker of molecular age, Arch Biochem Biophys. 350 (1) (1998) 61–71, https://doi.org/10.1006/abbi.1997.0492.

**Supplementary Material**

# Intra-operative Raman spectroscopy and *ex vivo* Raman mapping for assessment of cartilage degradation

Riana Gaifulina[a,b], Abigail D. G. Nunn[a], Edward R. C. Draper[c], Robin K. Strachan[d], Nathan Blake[e], Steven Firth[b], Geraint M. H. Thomas[e], Paul F. McMillan[b,*] and Jayesh Dudhia[a,*]

[a] Department of Clinical Science and Services, Royal Veterinary College, University of London, Hawkshead Lane, Hatfield, AL9 7TA, UK

[b] Department of Chemistry, University College London, Gordon Street, London, WC1H 0AJ, UK

[c] Department of Materials Science and Engineering, University of Sheffield, Mappin Street, Sheffield, S1 3JD

[d] Imperial College Healthcare NHS Trust, Charing Cross Hospital, Fulham Palace Road, London, W6 8RF, UK

[e] Department of Cell and Developmental Biology, University College London, Gower Street, London, WC1E 6AP, UK

[*]Corresponding author: jdudhia@rvc.ac.uk

**Supplementary Table 1: Details of specimens included in the *ex vivo* single-point spectroscopy study.**

ICRS grades G0 = grade 0, G1 = grade 1, G2/3 = grades 2 and 3 (combined group), G4 = grade 4 (late-stage osteoarthritis)

| Grade | Age (years) | Sex | Compartment location | Number of spectra recorded |
|---|---|---|---|---|
| **G0** | 36 | F | Medial condyle | 18 |
| | 59 | M | Medial condyle | |
| | 60 | M | Lateral condyle | |
| **G1** | 36 | F | Medial condyle | 22 |
| | 59 | M | Medial condyle | |
| | 66 | M | Medial condyle | |
| **G2/3** | 38 | F | Lateral condyle (G3) | 15 |
| | 44 | F | Medial condyle (G2) | |
| | 59 | M | Trochlear groove (G3) | |
| | 66 | M | Medial condyle (G2) | |
| **G4** | 59 | M | Medial condyle | 14 |
| | 68 | F | Medial condyle | |

**Supplementary Table 2: Details of clinical features of knee joints examined at arthroscopy during the in-clinic tests with visual grading of the cartilage lesions using the Outerbridge classification.**

M: Male, F: Female

| Patient | Age (years) | Sex | Outerbridge classification | Clinical description |
|---|---|---|---|---|
| **1** | 51 | F | Grade II | Medial femoral condyle erosions and medial meniscus tear |
| **2** | 48 | M | Grade II | Medial femoral condyle erosions and medial meniscus tear |
| **3** | 68 | M | Grade III | Lateral femoral condyle erosions and meniscus tear |
| **4** | 62 | F | Grade IV | Medial femoral condyle with late-stage osteoarthritis |

**Supplementary Table 3: Tentative assignments of Raman spectroscopic band for components of cartilage with various disease grades.**

The Raman spectra of tissue biomolecules are highly overlapping and peak positions are often reported with variabilities of ±1–5 $cm^{-1}$ due to experimental variability.

| Raman shift ($cm^{-1}$) | Assignment | Comments | Reference |
|---|---|---|---|
| 489 | Unknown | Characteristic of late stage cartilage disease, possibly molecular products of cartilage degradation (ICRS stage 4) | - |
| 531 | Disulphide stretching band in proteins | Associated with control and early OA cartilage disease (ICRS stages 1, 2 and 3). | [1] |
| 570 | Tryptophan | Associated with control and early OA cartilage disease (ICRS stages 1, 2 and 3). | [1] |
| 800 | Unknown | Characteristic of late stage cartilage disease, possibly molecular products of cartilage degradation (ICRS stage 4) | - |
| 831 | Tyrosine, collagen | Characteristic of late stage cartilage disease, possibly molecular products of cartilage degradation (ICRS stage 4) | [1, 2] |
| 856 | Collagen, $\nu$(C-C), proline | Associated with control and early OA cartilage disease (ICRS stages 1, 2 and 3). | [3-5] |
| 879 | Collagen, $\nu$(C-C), proline, hydroxyproline | Associated with control and early OA cartilage disease (ICRS stages 1, 2 and 3). | [3, 5] |
| 920 | Collagen, $\nu$(C-C), proline ring, hydroxyproline | Associated with control and early OA cartilage disease (ICRS stages 1, 2 and 3). | [3, 6, 4] |
| 939 | Collagen, $\nu$(C-C), proline in alpha helix | Associated with control and early OA cartilage disease (ICRS stages 1, 2 and 3). | [3-5] |
| 1003 | Ring breathing mode of phenylalanine | Associated with control and early OA cartilage disease (ICRS stages 1, 2 and 3). | [3, 5] |
| 1033 | Ring breathing mode of phenylalanine | Associated with control and early OA cartilage disease (ICRS stages 1, 2 and 3). | [3, 5] |
| 1063 | sGAGs, $\nu(SO_3^-)$ | Associated with control and early OA cartilage disease (ICRS stages 1, 2 and 3). | [6, 5] |
| 1098 | $\nu$(C-N) of proteins | Associated with control and early OA disease (ICRS stages 1, 2 and 3). | [3, 1] |
| 1245 | Collagen, amide III, $\delta$(N-H), random coil | Associated with control and early OA disease (ICRS stages 1, 2 and 3). | [3, 6, 5] |
| 1270 | Collagen, amide III, $\delta$(N-H), alpha helix | Associated with control and early OA disease (ICRS stages 1, 2 and 3). | [3, 5] |

| | | | |
|---|---|---|---|
| 1426 | sGAGs, $\nu(COO^-)$ vibration | Associated with control and early OA disease (ICRS stages 1, 2 and 3). | [3, 5] |
| 1451 | Collagen - other proteins, methylene deformation in biomolecules, $\delta$(C-H), in $CH_2/CH_3$ | Associated with control and early OA disease (ICRS stages 1, 2 and 3). | [3, 5] |
| 1622 | H-O-H vibrations of partially hydrogen-bonded (three-bonded) water | Characteristic of late stage cartilage disease (ICRS stage 4) | [7, 8] |
| 1645 | fully hydrogen-bonded (four-bonded) water | Characteristic of late stage cartilage disease (ICRS stage 4) | [7, 8] |
| 1702 | Carbonyl vibration of proteins | Characteristic of late stage cartilage disease (ICRS stage 4) | [1] |
| 2852 | $\nu(CH_2)$ and $\nu(CH_3)$, lipids | Associated with ICRS grade 1 cartilage disease | [2, 1] |
| 2874 | $\nu(CH_2)$ and $\nu(CH_3)$, lipids | Associated with ICRS grade 1 cartilage disease | [2] |
| 2917 | $\nu(CH_2)$ and $\nu(CH_3)$, lipids | Associated with ICRS grade 1 cartilage disease | [2] |
| 2951 | $\nu(CH_3)$, proteins | Characteristic of healthy control cartilage | [2] |
| 2995 | $\nu(CH_3)$, proteins | Characteristic of healthy control cartilage | [2] |

**Supplementary Fig. 1. Cartilage sampling and histology. a)** Samples were prepared from lesion sites (L) to include the lesion and the apparently normal cartilage at the margins (approximately 5 mm in size and full depth) as well as sites adjacent (A) and distal sites (D) to the lesions on either the medial or lateral femoral condyles of knee joints. **b)** Safranin O/Fast Green stained histological micrographs of cartilage sampled from normal specimens (grade 0), sites A (grade 1) and L (grade 2/3) and late osteoarthritic samples from total knee replacements (grade 4). Sulphated proteoglycans (sGAGs) stained increasingly weaker with disease grade.

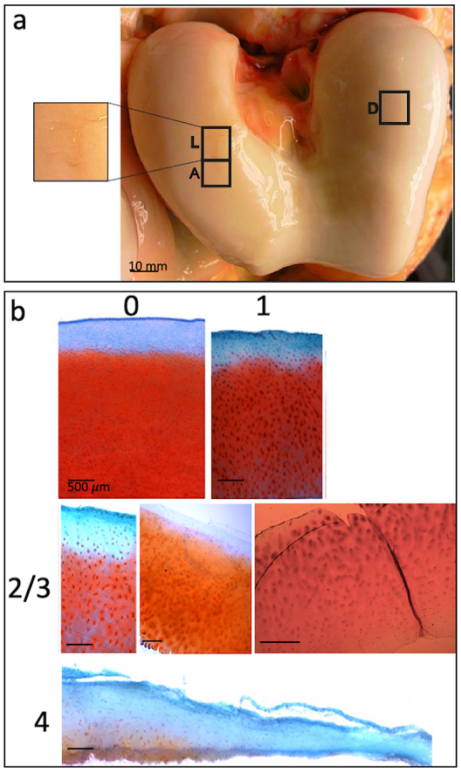

**Supplementary Fig. 2. Raman spectra in synovial fluid and water.** Spectra were acquired from normal cartilage samples as fresh tissue immersed in water ($H_2O$) or synovial fluid (Synovial) or in water after freezing at –80 °C and thawing (Frozen). No major differences were observed between the spectra over the entire spectral range shown. Subsequently, samples were stored frozen at –80 °C and Raman measurements were acquired with water immersion after thawing.

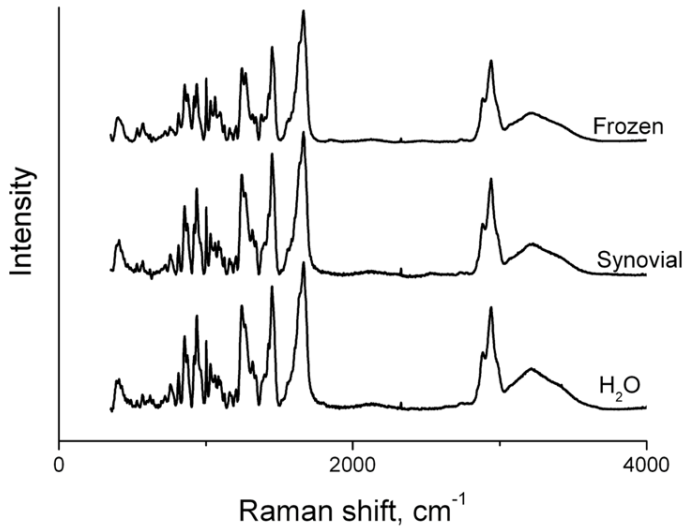

**Supplementary Fig. 3. Raman optical probe for clinical tests. a)** Schematic of the probe which consisted of a 6 mm (outer diameter) tube of 316L S16 steel with a main body length of 100 mm (annotated as 1), a threaded lens connector (2), a sapphire ball lens to focus the laser beam (3) and an endcap (4) incorporating a 4.5-mm-diameter sapphire window (5). The lens arrangement was designed such that the focal point was positioned at the exit of sapphire window, enabling focus-free use of the probe at arthroscopy. The lens and window were affixed in position with Loctite M31-CL epoxy adhesive. **b)** Photograph of notch filter assembly with the probe connected and an incoming fibre optic cable at the entry port (yellow tag). **c)** In-clinic application of the probe (left) and an image acquired during arthroscopy of the probe positioned abutting the cartilage in the knee joint (right). Here, the probe is set to scan macroscopically normal cartilage (in patient 1, in this representative example) distal to the eroding margin that can be seen towards the bottom right of the image. The probe was repositioned between measurements to allow spectra to be acquired from both macroscopically normal and eroding areas of cartilage

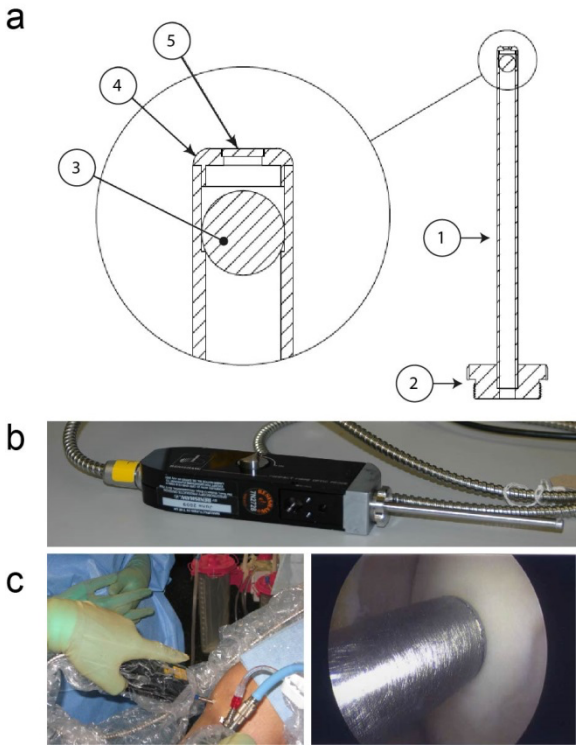

## References

1. Movasaghi Z, Rehman S, Rehman IU. Raman Spectroscopy of Biological Tissues. Applied Spectroscopy Reviews. 2007;42(5):493-541. doi:10.1080/05704920701551530.
2. Bergholt MS, Serio A, Albro MB. Raman Spectroscopy: Guiding Light for the Extracellular Matrix. Front Bioeng Biotechnol. 2019;7:303. doi:10.3389/fbioe.2019.00303.
3. Bonifacio A, Beleites C, Vittur F, Marsich E, Semeraro S, Paoletti S et al. Chemical imaging of articular cartilage sections with Raman mapping, employing uni- and multi-variate methods for data analysis. Analyst. 2010;135(12):3193-204. doi:10.1039/c0an00459f.
4. Mansfield JC, Winlove CP. Lipid distribution, composition and uptake in bovine articular cartilage studied using Raman micro-spectrometry and confocal microscopy. J Anat. 2017;231(1):156-66. doi:10.1111/joa.12624.
5. Pavlou E, Zhang X, Wang J, Kourkoumelis N. Raman spectroscopy for the assessment of osteoarthritis. Annals of Joint. 2018;3. doi: 10.21037/aoj.2018.09.10
6. Esmonde-White KA, Esmonde-White FW, Morris MD, Roessler BJ. Fiber-optic Raman spectroscopy of joint tissues. Analyst. 2011;136(8):1675-85. doi:10.1039/c0an00824a.
7. Walrafen GE, Blatz LA. Weak Raman bands from water. The Journal of Chemical Physics. 1973;59(5):2646-50. doi:10.1063/1.1680382.
8. Carey DM, Korenowski GM. Measurement of the Raman spectrum of liquid water. The Journal of Chemical Physics. 1998;108(7):2669-75. doi:10.1063/1.475659.